



Holocene paleoceanographic variability in Robertson Bay, Ross Sea, Antarctica: A marine record of ocean, ice sheet, and climate connectivity

Olivia J. Truax^{a,b,1,*}, Christina R. Riesselman^{a,b}, Gary S. Wilson^{b,c}, Craig L. Stevens^{d,e},
Rebecca L. Parker^{a,2}, Jae Il Lee^f, Robert M. McKay^g, Brad E. Rosenheim^h,
Catherine E. Ginnaneⁱ, Jocelyn C. Turnbull^{i,j}, Heung Soo Moon^f, Min Kyung Lee^f, Bob Dagg^{a,b},
Kyu-Cheul Yoo^f

^a Department of Geology, University of Otago, 360 Leith Street, Dunedin, 9016, New Zealand

^b Department of Marine Science, University of Otago, 310 Castle Street, Dunedin, 9016, New Zealand

^c University of Waikato, Private Bag 3105, Hamilton 3240, New Zealand

^d National Institute of Water and Atmospheric Research, 301 Evans Bay Parade, Hataitai, Wellington, 6021, New Zealand

^e Department of Physics, University of Auckland, Auckland, 1011, New Zealand

^f Korea Polar Research Institute, 26 Songdomirae-ro, Yeosu-gu, Incheon, 21990, South Korea

^g Antarctic Research Centre, Victoria University of Wellington, Wellington, 6012, New Zealand

^h University of South Florida College of Marine Science, 140 7th Avenue S, St. Petersburg, FL 33701

ⁱ Rafter Radiocarbon Laboratory, GNS Science, 30 Gracefield Road, Lower Hutt, 5010, New Zealand

^j CIRES, University of Colorado at Boulder, USA

ARTICLE INFO

Handling editor: A. Voelker

Keywords:

Antarctica
Holocene
Ross Sea
Sea ice
Circumpolar Deep Water
Paleoceanography
Diatoms
Sedimentology

ABSTRACT

Accelerating ocean-driven basal melting of Antarctic ice shelves in recent decades has implications for sea level rise and global overturning circulation. Here, we reconstruct oceanographic conditions at the confluence of the Ross Sea and the Southern Ocean by analyzing a multi-proxy Holocene marine sedimentary record collected from Robertson Bay. A ramped pyrolysis oxidation radiocarbon age-depth model provides a timeline for glacial behavior and oceanographic changes over the last 6700 years. The diatom assemblage, magnetic susceptibility, grain size, total organic carbon and nitrogen, trace elements, and bulk $\delta^{13}\text{C}$ are used as proxies for changing ocean and glacial conditions, which we interpret in the context of modern oceanographic measurements.

Our record shows evidence of persistent ice cover in the northwestern Ross Sea during the Antarctic mid-Holocene climate optimum (ca. 5 cal kyr BP). Based on this observation, we suggest that meltwater and iceberg discharge associated with ice sheet retreat in the Ross Sea region altered local oceanography during the mid-Holocene. The onset of modern style oceanographic conditions in Robertson Bay occurred at ca. 4 cal kyr BP. Stable late Holocene conditions in are punctuated by a period of enhanced polynya activity and upwelling of nutrient rich Circumpolar Deep Water ca. 0.8 cal kyr BP and an increase in the seasonal duration of sea ice after 0.7 cal kyr BP, during the Little Ice Age. The response of the marine environment in Robertson Bay to mid-Holocene ice sheet retreat and natural climate variability during the last millennium underscores the sensitivity of the Antarctic ice-ocean interface to projected changes in coming decades.

1. Introduction

Ice-ocean interactions play a key role in governing the stability of Antarctic ice sheets at their marine margins (Pritchard et al., 2012). Today, the incursion of relatively warm (>0 °C) Circumpolar Deep

Water (CDW) onto the continental shelf drives basal melt of the outlet glaciers at the northern margins of the East and West Antarctica ice sheets in response to a poleward contraction of the Southern Hemisphere Westerly Winds (Rignot et al., 2019; Spence et al., 2014). A number of observational and modeling studies show that meltwater

* Corresponding author.

E-mail address: olivia.truax@canterbury.ac.nz (O.J. Truax).

¹ Present address: School of Earth and Environment, University of Canterbury, Christchurch, New Zealand.

² Present address: Faculty of Environment, Science, and Economy, University of Exeter, Exeter, United Kingdom.

<https://doi.org/10.1016/j.quascirev.2024.108635>

Received 9 August 2023; Received in revised form 22 March 2024; Accepted 22 March 2024

Available online 26 April 2024

0277-3791/© 2024 The Authors. Published by Elsevier Ltd. This is an open access article under the CC BY license (<http://creativecommons.org/licenses/by/4.0/>).

discharge may further warm subsurface waters on the continental shelf, initiating a positive feedback with consequences for both the future stability of the ice sheet and ocean overturning circulation (Bronsele et al., 2018; Li et al., 2023; Miles et al., 2016; Silvano et al., 2018). However, our understanding of how changes in global mean climate state will affect the interplay between CDW upwelling and ice sheet stability is limited by sparse observations, present modeling capability, and the short duration of the instrumental period. The current generation of coupled global climate models are too coarse (i.e., approximately 1°) to capture the fine-scale processes such as local bathymetry, eddies, and polynyas that drive large regional differences in water mass circulation on the Antarctic continental shelf (Thompson et al., 2018). Further, the ~ 40 yr observational period routinely used to develop and evaluate predictive models is not long enough to characterize oceanographic variability on multi-centennial timescales (Jones et al., 2016; Thompson et al., 2018).

Paleoceanographic reconstructions from the Holocene (11,500 years ago to present) extend modern instrumental datasets and provide a unique opportunity to investigate the processes and feedbacks that drive the Antarctic ice-ocean system on multi-centennial to millennial timescales and during past intervals of ice sheet retreat. The Holocene was a dynamic period in the Antarctic. The East and West Antarctic ice sheets underwent rapid periods of retreat in the Ross Embayment, the continent's largest ice drainage basin, between 8 and 3.5 cal kyr BP (Halberstadt et al., 2016; Jones et al., 2020; McKay et al., 2016; Rhee et al., 2020; Siegert et al., 2019; Spector et al., 2017). Recent work shows that retreat was followed by a period of readvance and the ice sheets reached their modern configurations during the late Holocene (Neuhaus et al., 2021; Venturelli et al., 2020). Evidence of readvance is consistent with marine sediment cores, which record a baseline shift from a stable mid-Holocene climate optimum to a cooler, more variable, "Neoglacial" between 4.5 and 3 cal kyr BP (Ashley et al., 2021; Crosta et al., 2007; Denis et al., 2010; Domack et al., 2001; Johnson et al., 2021; Kim et al., 2018; Leventer et al., 1996; Peck et al., 2015). After the ice sheets stabilized, marine sediment and ice core records record multi-centennial variability in coastal sea ice, Antarctic Bottom Water (AABW) production, and CDW upwelling (Mezgec et al., 2017; Shevenell et al., 2011; Tesi et al., 2020; Xu et al., 2021).

The past two thousand years provides the most recent pre-industrial

examples of climate changes in the Antarctic. Fluctuations in temperature and wind patterns associated with the Medieval Climate Anomaly (MCA, ~ 950 to 750 cal yr BP) and Little Ice Age (LIA, ~ 500 –100 cal yr BP) intervals are documented in Antarctic ice and marine sediment cores and reproduced by paleoclimate model simulations (Bertler et al., 2011; Domack et al., 2001; Lüning et al., 2019; Truax et al., 2022). Paleoclimate reconstructions indicate a dipole pattern of temperature change in Antarctica between the MCA and LIA: cooling over most of mainland Antarctica and a warming trend along the eastern Antarctic Peninsula and in the eastern Ross Sea (Bertler et al., 2018; Lüning et al., 2019; Mulvaney et al., 2012). El Niño Southern Oscillation (ENSO) and the Southern Annular Mode (SAM) both drive dipoles in Antarctic temperatures and sea ice dynamics (Stammerjohn et al., 2008; Yuan, 2004). Previous research has suggested that multi-centennial trends in these modes of variability are a dominant control on climate in Antarctica during the MCA and LIA (Bertler et al., 2018; Koffman et al., 2023; Lüning et al., 2019). However, the relative influence of late Holocene orbital trends, mean-state changes in modes of climate variability (SAM and ENSO), and ice sheet discharge on late Holocene Antarctic oceanography are not yet well understood.

Here, we present a new reconstruction of primary productivity, glacial conditions, water mass circulation, and the seasonal duration of sea ice from a marine sediment core collected from Robertson Bay, a 40 km long north-south trending embayment located west of Cape Adare in the westernmost region of the Ross Sea (Fig. 1). Situated at the intersection between the Ross Embayment and the Southern Ocean, the Cape Adare region is influenced by processes occurring both along the continental margin and in the interior of the Ross Sea (Bowen et al., 2021). East of Cape Adare, cold, salty, High Salinity Shelf Water produced in Ross Sea polynyas mixes with fresher Antarctic Surface Water (AASW) and warmer upwelling-modified Circumpolar Deep Water (mCDW) to form Antarctic Bottom Water (AABW). Paleoclimate records from the western Ross Sea region are well placed to study the interplay between CDW upwelling, polynya processes, and sea ice dynamics through the Holocene (e.g. Mezgec et al., 2017; Tesi et al., 2020; Xu et al., 2021).

We examine mid-to-late Holocene paleoceanographic variability at the confluence of the Ross Sea and the Southern Ocean by analyzing a 6700 year multi-proxy record from Robertson Bay in the context of modern instrumental data. Our Robertson Bay record presents a unique

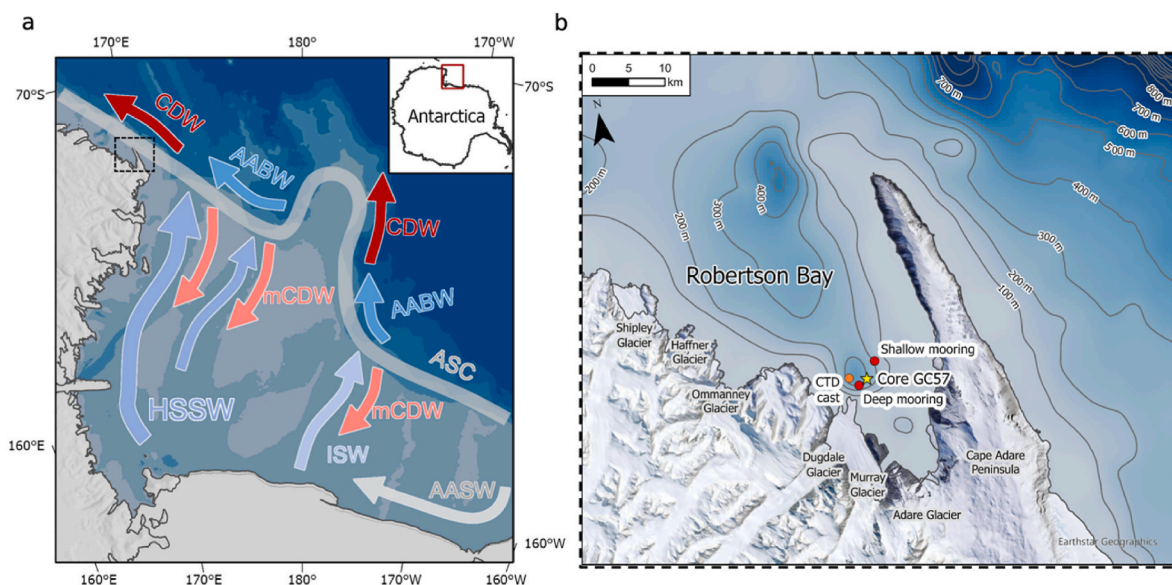


Fig. 1. Maps of a) the Ross Sea continental shelf highlighting major circulation features including Antarctic Surface Water, AASW (light blue); Circumpolar Deep Water, CDW (red); Modified Circumpolar Deep Water, mCDW (pink); Antarctic Bottom Water, AABW (dark blue), High Salinity Shelf Water (HSSW); and Ice Shelf Water (ISW). Grey line indicates the easterly flow of the Antarctic Slope Current (ASC). Dashed box shows the location of Robertson Bay with specific features highlighted in b) including the location of the RS15-GC57 core site (yellow), the location of the CTD cast (orange), and the shallow and deep moorings (red).

opportunity to reconstruct the impact of mid-Holocene ice sheet retreat (Halberstadt et al., 2016; Jones et al., 2020; Siebert et al., 2019; Spector et al., 2017) on a downstream region of the East Antarctic margin and assess the impact of orbital trends and large-scale modes of atmospheric variability (i.e. the Southern Annular Mode and El Niño-Southern Oscillation) on late Holocene sea ice dynamics and water mass exchange.

2. Materials and methods

2.1. Instrumental data

A salinity and temperature profile (CTD cast) was collected from Robertson Bay in early November of 2015 through a borehole in the sea ice (71°32.2672'S 170°03.5386'E) (Fig. 1; Fig. 2). Salinity and temperature of the water column were measured to a depth of 470 m using a Sea-Bird SBE 19 CTD with a Sea-Bird SBE 43 dissolved oxygen sensor and a Wetlabs Wetstar WS3S fluorometer on the downcast. Two Sea-Bird SBE 37-SMP-ODO CTDs mounted on hydrographic moorings were deployed in the interior of the Bay at depths of 45 m, 53 m, and 302 m ("shallow" and "deep" respectively, Fig. 1) in January 2015 during KOPRI cruise ANA05B and recovered in January of 2017 (Fig. 3). Salinity, potential temperature, and dissolved oxygen measurements from the CTD cast are corrected using the mooring data (Supplementary Data). A weather station measuring wind direction, wind speed, and air temperature was also installed on the Cape Adare ridge and we present one year of continuous measurement starting in November 2015. Modern sea ice dynamics (2003–2022) were examined using satellite data from Terra MODIS and Aqua MODIS and accessed via NASA Worldview images (Fig. 3) (NASA Worldview; <https://worldview.earthdata.nasa.gov/>).

2.2. Sampling and subsampling

Gravity core RS15-GC57 was collected from Robertson Bay by the R/V *Araon* during the ANA05B Cruise in 2015 (71°32.27'S, 170°03.54'E; 344 m water depth), recovering 570 cm of sediment. Shipboard observations indicate intact recovery of the core top. The core was split,

imaged, X-rayed, and described at the Korea Polar Research Institute (KOPRI) in August of 2015. U-channels were collected and sub-samples for geochemical and quantitative diatom analysis were taken at 5 cm increments to enable high-resolution paleoenvironmental reconstruction. All subsamples were frozen and freeze-dried before analysis.

2.3. Proxy analysis

Samples were homogenized using an agate mortar and pestle for geochemical analysis. Biogenic silica (wt% BSi) was measured at the University of Otago using an alkaline extraction spectrophotometric method modified from Strickland and Parsons, 1972 and Mortlock and Froelich (1989). Replicates were measured after every 10th sample, and one blank and one internal standard were analyzed with every analytical run. The average standard deviation of the 31 replicates is 0.25%.

Sample preparation for total organic carbon (TOC) and $\delta^{13}\text{C}$ analysis of bulk decalcified sediment was completed at the University of Otago. Thirty milligrams of sediment was weighed into silver capsules. The sediment was acidified progressively with four additions of 6% sulphurous acid (H_2SO_3) (40 ml x1; 60 μL x 2; 80 μL x 1) to remove carbonate and analyzed using a Carlo Erba NA1500 Series 2 Elemental Analyzer interfaced with a DeltaPlus isotope ratio mass spectrometer via a ConFlo II interface at the Stanford University Stable Isotope Laboratory. The average standard deviation across 35 replicates is 0.20‰ for $\delta^{13}\text{C}$ and 0.03% for TOC. Total nitrogen (TN) concentrations were measured with an Organic Elemental Analyzer (FLASH, 2000 NC Analyzer) at KOPRI. Volume-normalized magnetic susceptibility was measured at 1 cm increments on a u-channel using a 30 mm Barrington loop sensor (MS2C) on the University of Otago's Geotek multi-sensor core logger.

Grain size data were analyzed at 5 cm intervals at KOPRI on samples treated with H_2O_2 and HCl to remove organic matter and CaCO_3 , respectively. Coarse fractions (>63 μm) were analyzed with a set of sieves to determine the distribution of gravel to very fine sand grain sizes. Grain size distribution of finer fractions (<63 μm) were analyzed using a Micrometric Sedigraph III 5120. The grain size statistics follows the methods of Folk and Ward (1957) and lithological classification scheme follows that of McKay et al. (2019). Diatomaceous opal in the

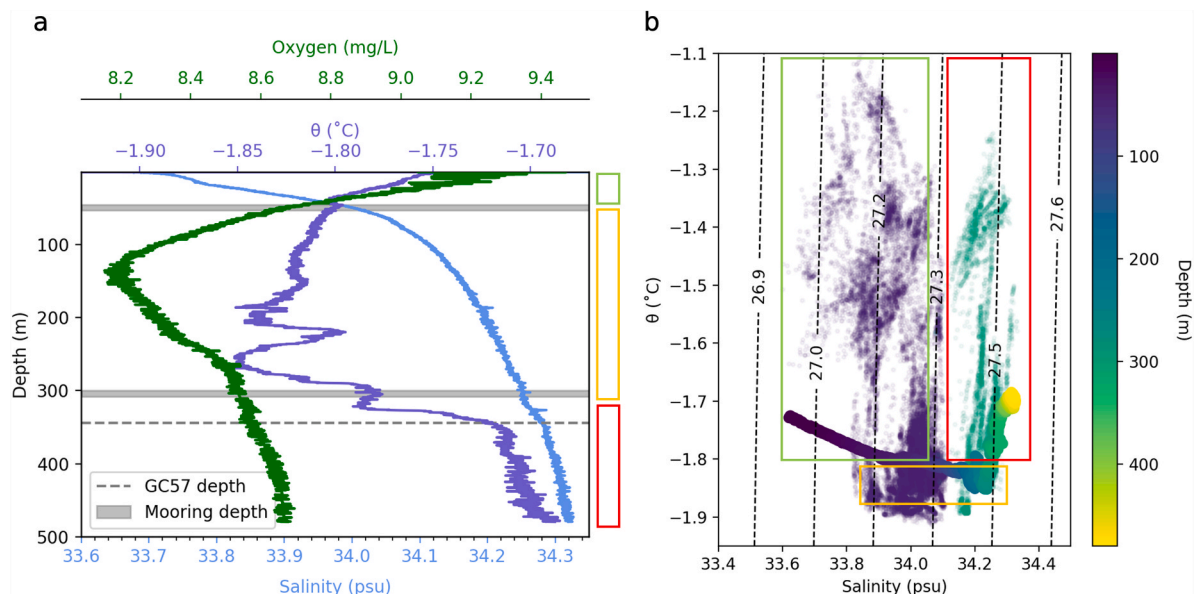


Fig. 2. Characteristics of water masses in Robertson Bay; a) vertical profile from the CTD cast taken in November of 2015 showing oxygen concentration (green), potential temperature (θ ; purple), and salinity (blue); grey bars indicate the depths of the shallow and deep moorings, dashed line shows depth of the GC57 core site. Colored boxes indicate warmer and fresher Antarctic Surface Waters (pale green), colder remnant Winter Water (orange), and warmer heavily modified Circumpolar Deep Water present at depth (red); and b) Potential temperature (θ) versus salinity from the CTD cast (November 2015) and moorings (February 2015 to February 2016). Dashed lines show lines of neutral density; colored boxes indicate water masses identified in the main text.

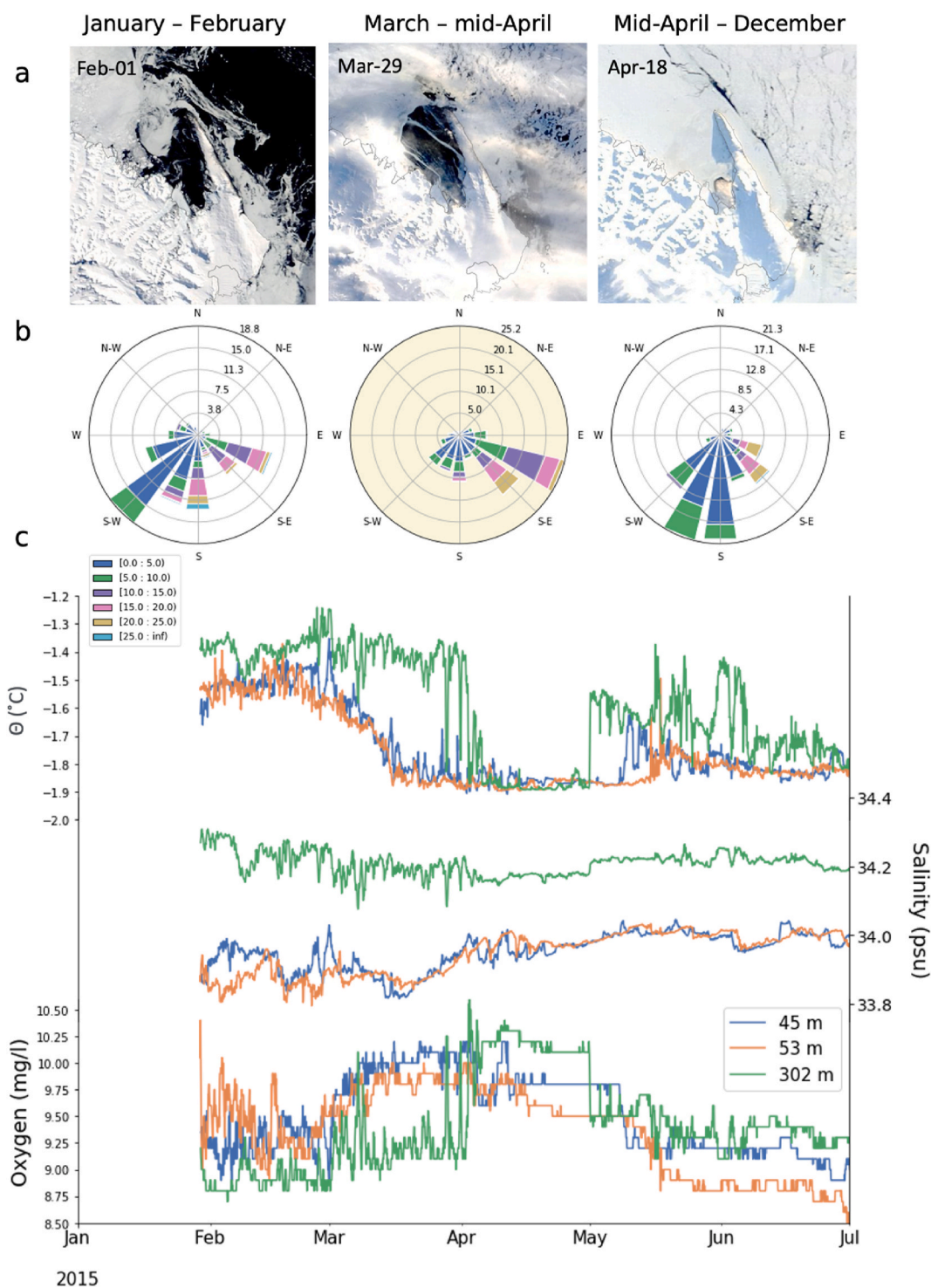


Fig. 3. Synthesis of modern conditions in Robertson Bay; a) satellite photos of Robertson Bay sea ice dynamics in austral summer, autumn, and early winter of 2015 (NASA Worldview; <https://worldview.earthdata.nasa.gov/>); b) prevailing winds (January and February, March to April 15th, and April 15th through December) by direction, strength (meters per second), and frequency along the Cape Adare Ridge in 2016 (see also [Supplementary Data](#)); c) oceanographic data from Sea-Bird SBE 37-SMP-ODO CTDs deployed on shallow (45 and 53 m) and deep (302 m) hydrographic moorings.

core is relatively low (8–15%; Section 3.3) compared to other Holocene Antarctic sediments (e.g. 30–60%, [Ashley et al., 2021](#)), and therefore biogenic opal will only represent a subordinate signal within the grainsize distributions, with the greatest influence in the fine silt size range ([McKay et al., 2022](#); [Warner and Domack, 2002](#)). Bromine (Br), titanium (Ti), magnesium (Mn), and iron (Fe) counts were measured on split core using ITRAX XRF Core Scanner with Mo X-ray tube, 1-mm step

size, and 5-s exposure time at 30 kV and 30 mA at KOPRI.

Settled slides for quantitative diatom analysis were prepared at the University of Otago using the method of [Warnock and Scherer \(2015\)](#). Diatom census counts were carried out using an Olympus BX41 microscope using a 63 x objective and 10x eyepiece; a minimum of 300 valves per sample were counted to reach a statistically representative census. Pennate diatoms and *Eucampia antarctica* were counted as 'one half' for

each apex or elevation identified, and the total count was divided by two. Each centric valve was counted as 'one' if the margin and central area were present. The relative abundance of each diatom species was determined as a percentage of total diatom valves counted for each sample. Absolute diatom abundance was calculated following Warnock and Scherer (2015).

Environmental inferences from proxy archives are made according to the literature summarized in Table 1.

2.4. Statistical analysis

Principal components analysis (PCA), was carried out on proxy archives using the Scikit-learn Python module (Pedregosa et al., 2011). Data were resampled to 5 cm binned averages prior to PCA analysis and linear correlations between records were calculated using the pandas Python module (Reback et al., 2020).

2.5. Age model

The age model of core RS15 – GC57 is based on accelerator mass spectrometry (AMS) radiocarbon measurements from eight core depths. Three horizons yielded sufficient carbonate from foraminifera and a shell fragment for radiocarbon measurement and six horizons were radiocarbon dated using the ramped pyrolysis oxidation (RPO) method (Rosenheim et al., 2008). Radiocarbon preparation by RPO reduces contamination from ancient detrital sources by exploiting the thermochemical stability differences between the fresh autochthonous, acid-insoluble organic (AIO) material and the diagenetically stabilized allochthonous AIO material (Rosenheim et al., 2013b; Subt et al., 2016). During RPO, a pretreated sediment sample is gradually heated at 5 °C/min up to 1000 °C under a stream of helium, pyrolyzing organic material according to its thermochemical stability. The resultant volatile compounds are oxidized to CO₂ over Pt, Ni, and Cu wires with ultra-high purity oxygen gas and fractions are cryogenically collected according to the temperature at which the volatiles were evolved. The separation of samples into several fractions (termed splits) for radiocarbon dating produces a spectrum of ages. Generally, the least thermochemically stable material, evolved at lowest pyrolysis temperature, is youngest, while the most thermochemically stable material, evolved at highest pyrolysis temperature, is oldest (Rosenheim et al., 2013b; Subt et al., 2016).

Samples from four depths (0, 180, 455, and 560 cm) were pretreated for RPO at the University of Otago following Rosenheim et al. (2008). Samples were acidified for 24 h in 1N HCl to remove any carbonate material present, dried at 60 °C, and stored in pre-combusted vials until analysis. RPO and CO₂ fraction collection was performed at the College of Marine Science, University of South Florida (USF), United States of America. RPO pretreatment and CO₂ fraction collection were performed on two additional samples (380 and 505 cm) at the Rafter Radiocarbon Lab (RRL) AMS facility at GNS Science, New Zealand. These samples

were acidified in 1N HCl for 18 h to remove any carbonate material present, dried at 50 °C, and stored in pre-combusted vials until analysis. RPO and CO₂ fraction collection at RRL was carried out using protocols adapted from Rosenheim Laboratory at the USF (Rosenheim et al., 2013b; Ginnane et al., 2024). All radiocarbon measurements were performed at the RRL AMS facility following standard graphitization and AMS measurement protocols (Turnbull et al., 2015; Zondervan et al., 2015), corrected for blank contamination by the procedures outlined in Fernandez et al. (2014), and modified for the systems at USF and RRL during the time of analysis (Supplementary Data).

3. Results

3.1. Modern environment

Robertson Bay is a protected embayment close to the shelf break at the western confluence of the Ross Sea and the Southern Ocean (Fig. 1). Outlet glaciers from the Transantarctic Mountains terminate into the bay. Robertson Bay has a sill at approximately 200 m, and the inner bay is divided into inner and outer basins.

A CTD cast taken through a hole in the sea ice in November 2015 provides a snapshot of the complex water column structure in Robertson Bay (Fig. 2). From the surface, potential temperature (θ) and oxygen decrease and salinity increases. Oxygen concentration reaches a minimum of 8.2 mg/L ca. 135 m and increases with depth. A colder water mass (<-1.8 °C) between 50 and 300 m overlies warmer waters (>-1.8 °C), and the salinity gradient sustains water column stability.

Robertson Bay has typically been sea ice-free from mid-January to mid-March during the satellite era (Fig. 3) (NASA Worldview; <https://worldview.earthdata.nasa.gov/>). Surface waters in the embayment warm, freshen, and become more oxygenated over the course of the summer open water season. Sea ice advances from the north towards the coast in late March, and pack ice is typically present in the bay by the end of March. Sea ice coverage in the bay can change rapidly due to wind. Strong southeasterly winds form a polynya at the head of Robertson Bay in April of most years (Fig. 3). Shallow (45 and 53 m) and deep (302 m) moorings show that the cold, oxygenated water mass formed by brine rejection broke down the salinity gradient in the embayment in April of 2015, ventilating the inner basin (Fig. 3). The water mass produced during wintertime convection in Robertson Bay in 2016 is close to the surface freezing point (~-1.8 °C) and fresher than Dense Shelf Waters formed in the Ross Sea, which have a salinity of less than 34.5 psu (Orsi and Wiederwohl, 2009). When polynya activity ceased and fast ice conditions were established in early May 2015 warmer CDW upwelling along the East Antarctic margin intruded over the sill (cf. Williams et al., 2010). This warmer, saltier, oxygen-depleted water mass was modified by the colder, fresher, and more oxygenated waters within the embayment (Fig. 3).

We synthesize our interpretation of the mooring, satellite data, and CTD cast data to characterize three endmembers of Antarctic Surface

Table 1
Summary of the relationships between sedimentary proxies and environmental conditions.

Proxy	Proxy interpretation
Magnetic susceptibility (MS)	The relative contribution of terrigenous input and siliceous diatom productivity (Brachfeld and Banerjee, 2000).
Weight percent biogenic silica (wt% BSI)	The relative contribution of terrigenous input and siliceous diatom productivity (DeMaster et al., 1996)
Total organic carbon (TOC)	Primary productivity and/or anoxia (Domack and Ishman, 1993)
Total nitrogen (TN)	Primary productivity (e.g. Kim et al., 2018)
Absolute diatom abundance (ADA)	Siliceous diatom primary productivity (Leventer, 1992).
The ratio of bromine to titanium (Br/Ti)	Primary production (Agnihotri et al., 2008; Ziegler et al., 2008).
Grain size	The grain size of fine sands and muds are a function of current strength and settling velocity (Johnson et al., 2021)
$\delta^{13}C$	Biologic productivity and water mass circulation (Gibson et al., 1999; Villinski et al., 2000)
The ratio of <i>Chaetoceros</i> spp. to <i>Chaetoceros</i> resting spores (CRS)	Nutrient-rich, mixed, surface waters, mCDW influence (Beans et al., 2008; Leventer et al., 1996)
The relative abundance of <i>Fragilariopsis curta</i>	Persistent spring sea ice; sea ice melt-water stabilized upper water column (Cunningham and Leventer, 1998; Leventer and Dunbar, 1996)
The ratio of manganese to iron (Mn/Fe)	Sediment redox conditions (high Mn/Fe ratios indicate oxic conditions) (Naeher et al., 2013)

Water in Robertson Bay (Orsi and Wiederwohl, 2009). The upper water column consists of warmer (>-1.8 °C) and fresher (<34.0 psu) surface waters. This water mass warms throughout the summer season and freshens due to melt from sea ice and East Antarctic outlet glaciers, which terminate into the embayment (Fig. 1; Fig. 2; Fig. 3). Saltier (>34.0 psu) and colder (<-1.8 °C) waters occupy mid-depths and are likely a remnant of the water mass formed during autumn sea ice production (cf. Silvano et al., 2017). This remnant winter water overlies a warmer (>-1.8 °C) and saltier (>34.1 psu) water mass produced by mixing between the cold oxygenated water mass produced within Robertson Bay during autumn polynya activity and warmer, saltier mCDW located off the continental shelf in the Cape Adare region (Gordon et al., 2015).

3.2. Sedimentary chronology

The age model of core RS15-GC57 is based on AMS radiocarbon dates for eight stratigraphic horizons (Table 2). In core RS15-GC57, the ages of the second measured RPO CO₂ fraction (split 2, varying temperature ranges but typically 300–350 °C) are younger than the first measured fraction (split 1, typically up to ~ 300 °C) and exhibit age differences between 130 and 810 ¹⁴C yrs (Table 2; Supplementary Data). The second split is also found to trend slightly younger than the first split in other diatom-rich Holocene sediment cores collected from the western Ross Sea (Ginnane et al., 2024; Parker, 2017). Younger radiocarbon age trends in the second split imply that older, potentially translocated or naturally degraded, labile material volatilized at low temperatures is contaminating the lowest temperature split (Ginnane et al., 2024). This behavior appears to be unique to Ross Sea sediments; generally, older organic matter has been associated with higher temperature splits in Antarctic margin sediments (Rosenheim et al., 2008, 2013b; Subt et al., 2016, 2017; Venturelli et al., 2020) and elsewhere in the world (Bianchi et al., 2015; Gaglioti et al., 2014; Rosenheim et al., 2013a; Rosenheim and Galy, 2012; Schreiner et al., 2014; Vetter et al., 2017; Williams et al., 2015; Zhang et al., 2017). The only other examples of older samples volatilizing at lower temperatures using this method come from sediment contaminated with petroleum from Miocene-aged source rock

(Adhikari et al., 2016; Pendergraft et al., 2013; Pendergraft and Rosenheim, 2014). The second RPO split at 180 cm (collected between 316 and 382 °C) is more consistent with the carbonate dates at 180 cm (2770 ± 65 and 2642 ± 26 ¹⁴C yrs BP respectively; Supplementary Data) than the first split, which contained carbon volatilized below 316 °C. Better agreement between the second RPO split at 560 cm and a carbonate date at 567 cm (7320 ± 100 and 6914 ± 152 ¹⁴C yrs respectively) provides further indication that split 2 provides a more robust age constraint, supporting the conclusion that a higher proportion of pre-aged organic matter is volatilizing in the lowest temperature interval (Supplementary Data).

The final age-depth model for core RS15-GC57 was built on eight dated horizons (Fig. 4). Calibration of ¹⁴C dates to calendar years before present (cal yr BP) was performed using the Bchron R package (Haslett and Parnell, 2008) and the Marine20 calibration curve, which includes a time-varying global reservoir age of ~ 600 years, R(t) (Heaton et al., 2020). The core top RPO radiocarbon age of 1310 ¹⁴C year BP (1375 years before core collection 2015 CE) is adopted as the most robust estimate of the local ocean reservoir effect (ΔR) and any remaining contamination by detrital carbon (DC) in RPO dates. We adopt an uncertainty of ± 150 years to account for the error in the core top radiocarbon date (± 65 years, Table 2) combined in quadrature with Holocene reservoir variability in the Ross Sea region (± 137 years, Gao et al., 2022; Hall et al., 2010). We also adopt a global marine reservoir, R(t), of 603 years, the most recent available estimate from the Marine20 calibration curve, which yields a total local radiocarbon correction ($\Delta R + DC$) of 772 years (Heaton et al., 2020).

We employ a constant local radiocarbon correction with the caveat that variable upwelling of mCDW in the northern Ross Sea during the Holocene (e.g. Xu et al., 2021) likely drives substantial radiocarbon reservoir variability because mCDW is depleted in ¹⁴C relative to the global marine radiocarbon reservoir (Heaton et al., 2020, Heaton et al., 2023; King et al., 2018). Though precise calibrations that account for polar ΔR variability are not yet available, future efforts to develop and validate high latitude curves will be essential to constrain the timing of Antarctic paleoceanographic change during the Holocene (Heaton et al., 2023).

Table 2

Dated horizons in core RS15-GC57. Dates included in the final calibrated age model highlighted in grey. Room temperature is abbreviated to RT.

Depth (cmbsf)	Type of date	Temp. range (°C)	RPO lab	NZA #	Conventional Radiocarbon Age (¹⁴ C yr BP)	Calibrated age range (95% CI, cal yr BP)	
						Min	Max
0-1	RPO split 1	RT - 297	USF	62683	1440 \pm 80		
	RPO split 2	297-341	USF	62684	1310 \pm 60	-71	49
180-181	RPO split 1	RT - 316	USF	62685	3360 \pm 140		
	RPO split 2	316 - 382	USF	62686	2770 \pm 85		
	Carbonate (shell fragment)	-	-	61835	2642 \pm 26	824	1430
220-222	Carbonate (shell fragment)	-	-	61836	2885 \pm 26	1771	1894
380-381	RPO split 2	300 - 380	RRL	72390	4012 \pm 88	2416	3292
455-456	RPO split 1	RT - 328	USF	62696	4910 \pm 120		
	RPO split 2	328-403	USF	62697	4650 \pm 110	3373	4884
505-506	RPO split 2	270 - 370	RRL	72389	5888 \pm 44	4823	5518
560-561	RPO split 1	RT- 284	USF	62691	8130 \pm 170		
	RPO split 2	284 - 327	USF	62692	7320 \pm 100	5809	6733
	Carbonate (benthic and planktic foraminifera)	-	-	61894	6914 \pm 152	6169	7049

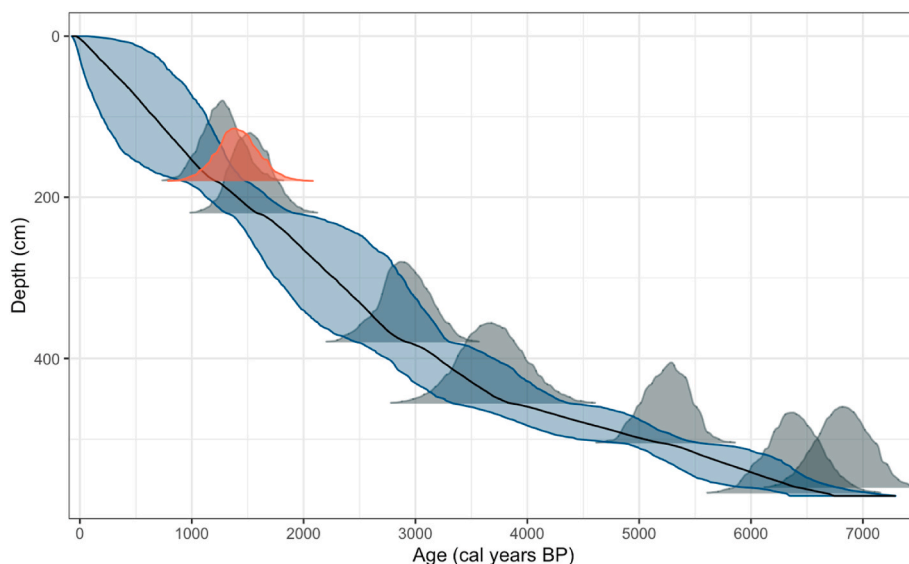


Fig. 4. Calibrated age model for core RS15-GC57. Median age–depth relationship is in black, with 95th percentile range shaded in blue. Calibrated radiocarbon dates included in the age model are shown in grey. The date at 180 cm excluded from the final age–depth model is highlighted in red.

A local radiocarbon reservoir age of 1375 ± 150 years in Robertson Bay is consistent with the Holocene radiocarbon reservoir age of 1000–1300 years in the Southwestern Ross Sea calculated from the difference between U/Th and ^{14}C in corals (Hall et al., 2010) and measurements from other regions of the Antarctic margin (Ó Cofaigh et al., 2014 and references therein). We adopt our locally calculated radiocarbon offset ($\Delta R + DC$) of 772 ± 150 years to generate our age model, noting that it is statistically indistinguishable from the weighted average ΔR for the Ross Sea region 609 ± 137 (Gao et al., 2021). Agreement between the locally calculated reservoir off set for core GC57

and the regional average Ross Sea ΔR provides further evidence that the core top was recovered intact and RPO mitigates contamination from ancient detrital sources, which influence bulk radiocarbon dates from coastal sediment cores in the Ross Sea (e.g. Mezgec et al., 2017; Tesi et al., 2020).

3.3. Multi-proxy marine archive

Principal component analysis (PCA) was used to determine the relationship between proxy indicators of primary production,

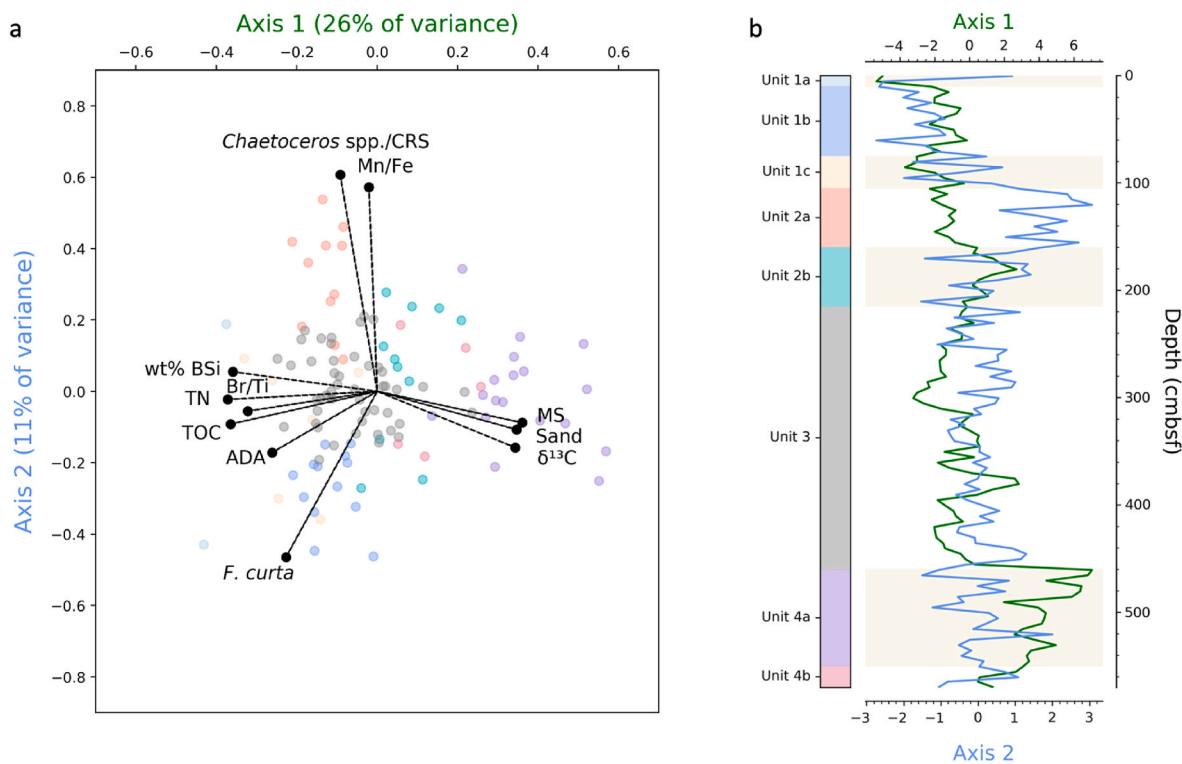
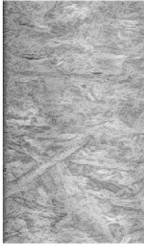
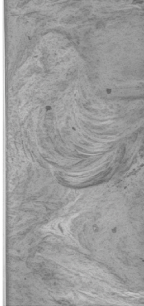


Fig. 5. Principal Component Analysis (PCA) results from Robertson Bay environmental proxies. Axis 1 is dominated by proxies for terrigenous versus biogenic sedimentation, and axis 2 is dominated by proxies for sea ice, nutrient concentration, and polynya activity (see details in Table 4). a) Ordination bi-plot of variable loadings for the first two axes of the PCA; b) stratigraphic plot of component scores for Axes 1 and 2.

Table 3
Sedimentary facies descriptions and interpretations.

Facies	Core Depth (cmbsf)	X-radiograph	Lithology and Sedimentary features	Interpretation
M _{BSi}	0–403		Pervasively bioturbated biosilica-bearing muds with dispersed clasts (DO). Moderately high wt% biogenic silica (10–14%), TOC content (>0.5%)	Pelagic sedimentation with hemipelagic suspension settling (Domack et al., 1999; Smith et al., 2019). Occasional ice rafted debris. Diatom assemblage is consistent with seasonal fast ice overlying the site, but with sea ice breakout in summer (this study; section 3.1).
SM _L	403–570		Laminated sandy mud, physically intermixed with bioturbated mud containing dispersed clasts (wt% biogenic silica <10%). Deformed mm-scale fine sands to coarse silts laminae, that commonly have sharp upper and lower contacts. Intermixing characterised by discrete “blocks” of the differing lithologies, with curvate, cross-cutting lower contacts.	Hemipelagic suspension settling. Lower biogenic silica content likely represents increase ice cover (perennial sea ice or small cavity ice shelf) over site (reduced productivity) (Domack et al., 1999; Hemer and Harris, 2003). Outsized clasts are present, but rare - indicative of deposition beneath sea ice or a small cavity ice shelf containing basal debris proximal to grounding line (Domack et al., 1999; Hemer and Harris, 2003; McKay et al., 2008). Sorted, fine sand/coarse silt laminae suggest presence of moderately-strong bottom current to winnow/prevent suspension settling of muds (McKay et al., 2008; Smith et al., 2019; Johnson et al., 2021). Intermixing is consistent with post-depositional scouring/turbation by icebergs (Hillenbrand et al., 2014), or glaciotectonic deformation in a proglacial setting (Evans and Benn, 2014).

glaciomarine sedimentation, and ocean conditions in core RS15-GC57 (Fig. 5). The first two axes of the PCA account for 26% and 11% of the variance in the proxy records respectively. Magnetic susceptibility (MS), weight percent biogenic silica (wt% BSi), Br/Ti ratio, TN, and $\delta^{13}\text{C}$ are strongly correlated ($R > \pm 0.57$, Supplementary Data) in core RS15-GC57 and dominate the variance captured by axis 1 of the PCA. Axis 2 of the PCA reflects the inverse relationship between the relative abundance

of the diatom *Fragilariopsis curta* and both the ratio of vegetative frustules of the diatom genus *Chaetoceros* to *Chaetoceros* resting spores (CRS) and the Mn/Fe elemental ratio. Changes in the PCA were used to identify four stratigraphic intervals: Unit 1 (0–105 cm), Unit 2 (105–215 cm), Unit 3 (215–460) and Unit 4 (460–570) (Fig. 5). Two lithofacies are identified in the core: pervasively bioturbated biosilica-bearing muds (0–403 cm) and laminated sandy mud (403–570 cm) (Table 3).

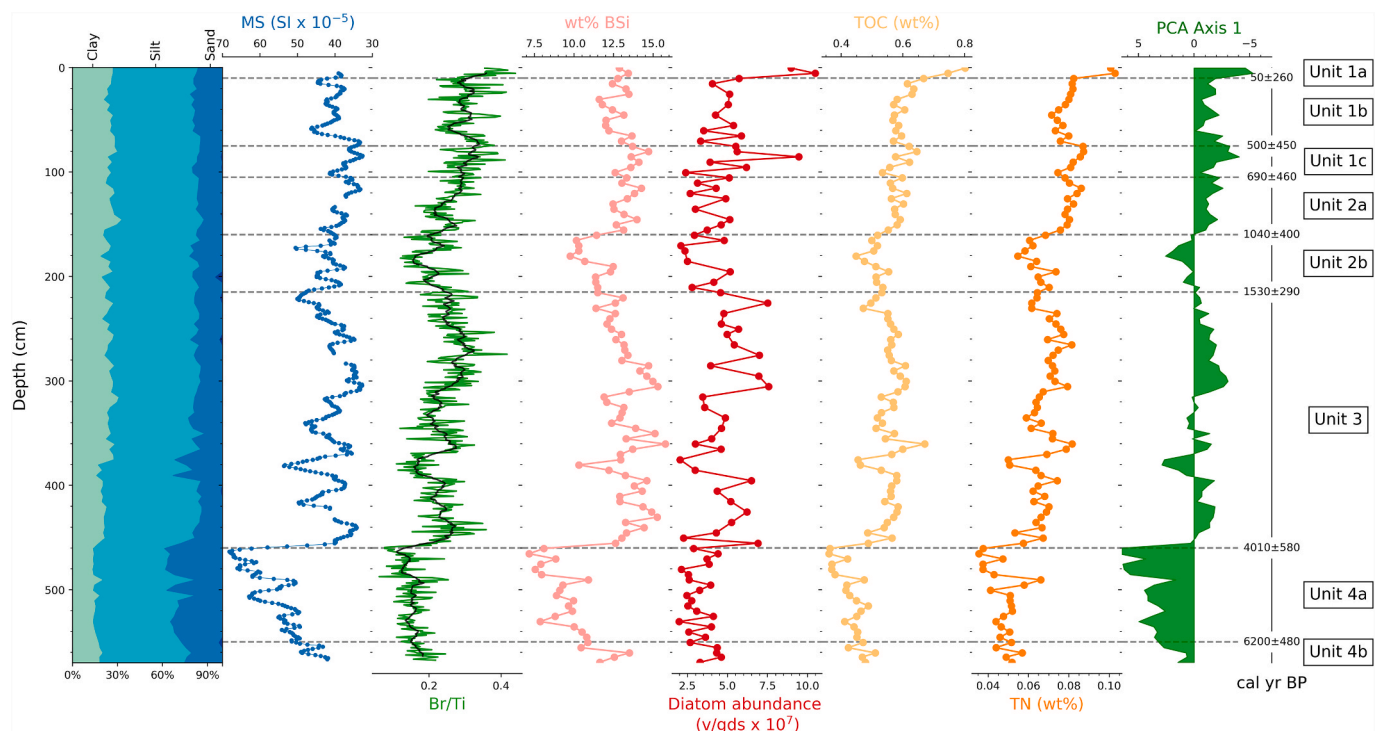


Fig. 6. RS15-GC57 downcore profiles of proxies for terrigenous and biogenic sedimentation including grain size; magnetic susceptibility (MS; SI); bromine to titanium ratio (Br/Ti), weight percent biogenic silica (wt% BSi), absolute diatom abundance (ADA; valves per gram dry sediment), total organic carbon (TOC; %), total nitrogen (TN; %), and axis 1 of the PCA, which is dominated by variance in these proxies (Fig. 5). Dashed lines show boundaries between units and subunits identified based on the PCA with calibrated ages and uncertainties from the age-depth model.

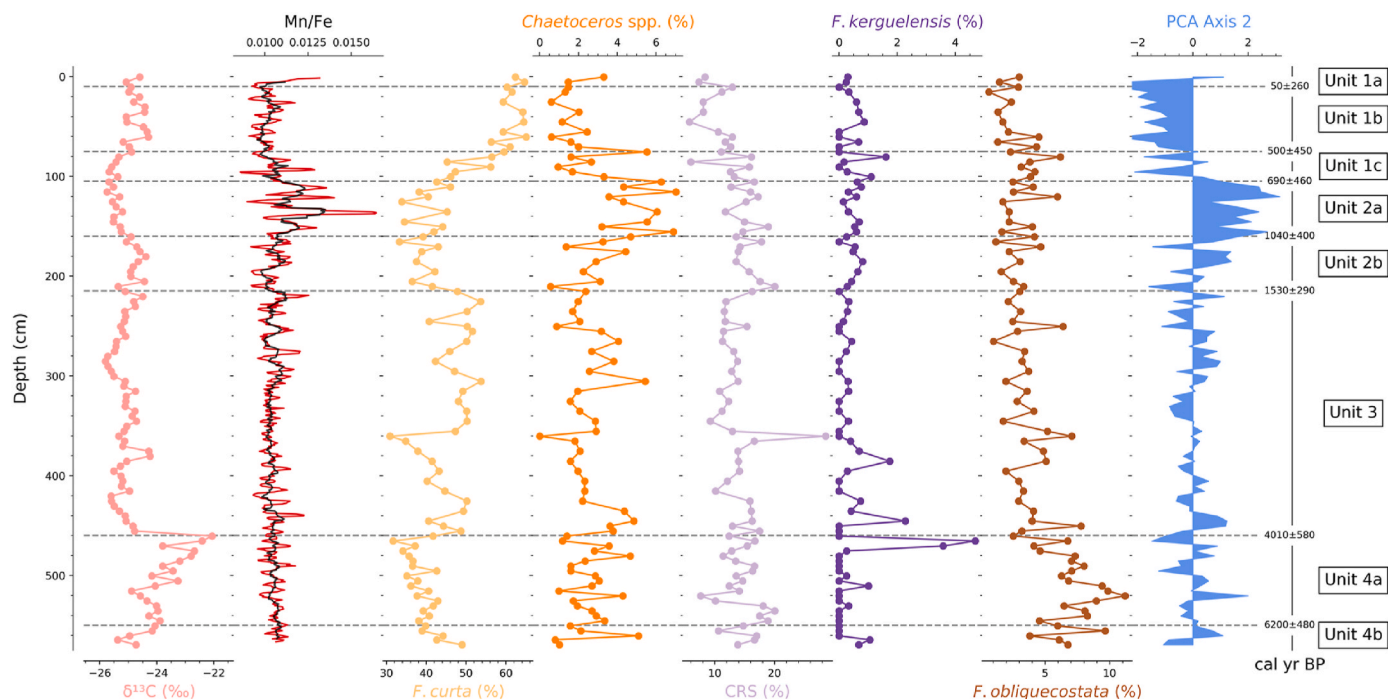


Fig. 7. RS15-GC57 downcore profiles of proxies for oceanographic and sea ice dynamics including stable isotopes of carbon ($\delta^{13}\text{C}$), manganese to iron ratio (Mn/Fe), the relative abundances of *F. curta*, *Chaetoceros* spp., *Chaetoceros* resting spores (CRS), *F. kerguelensis*, and *F. obliquecostata*, and axis 2 of the PCA, which is dominated by variance in *F. curta*, *Chaetoceros* spp., and CRS abundance and Mn/Fe ratio. Dashed lines show boundaries between units and subunits identified based on the PCA with calibrated ages and uncertainties from the age-depth model.

The uppermost unit of core RS15-GC57, Unit 1 (0–105 cm), is characterized by *F. curta* relative abundance greater than 50% and lowest down core abundances of *Fragilariopsis sublinearis* (<5%) and *Thalassiosira antarctica* (0–2%) (Fig. 6; Supplementary Data). The CRS relative abundance, Br/Ti ratio, TOC, and ADA are higher in the upper section of Unit 1, Unit 1a, and lower in Unit 1b and 1c (Fig. 7). *Fragilariopsis curta* abundance is higher (>65%) in Unit 1b than Unit 1c (50%). $\delta^{13}\text{C}$ also shifts from more positive values in Unit 1b to more negative values at the top of Unit 2.

The relative abundance of *F. curta* drops below 50% in Unit 2 (105–215 cm) and the diatom assemblage is further characterized by the highest down core abundances of *Fragilariopsis sublinearis* (Fig. 7; Supplementary Data). The upper section, Unit 2a, is distinguished from the lower Unit 2b by a higher ratio of *Chaetoceros* spp. to CRS and the highest Mn/Fe values measured in RS15-GC57. ADA, Br/Ti, TOC, TN, and wt% BSi are lower in Unit 2b and $\delta^{13}\text{C}$ and MS are higher; this inverse relationship is captured by axis 1 of the PCA. Sedimentary accumulation in Unit 2b lower (~1 mm/yr) than Unit 2a and Unit 1 (>1.5 mm/yr) (Supplementary Data).

Unit 3 (215–455 cm) is defined by a return to higher *F. curta* abundance (>50%). Wt% BSi and Br/Ti shift toward higher values between 170 cm and 305 cm and are more variable between 305 cm and the base of Unit 3, 455 cm. Although *F. curta* abundance is generally above 50% throughout the unit, a transient interval of lower in *F. curta* relative abundance (40%), lower wt% BSi, ADA, TOC, and Br/Ti, and elevated MS and $\delta^{13}\text{C}$ is evident ca. 380 cm. A transient increase in the relative abundance of CRS is also evident at 380 cm (Fig. 7). The transition from pervasively bioturbated diatom-bearing mud to laminated sandy mud occurs within Unit 3 at 403 cm (Table 3); laminae are particularly pronounced between 405 and 420 cm. A stepwise shift toward higher Br/Ti, ADA, wt% BSi, and TOC and lower MS, sand abundance, and $\delta^{13}\text{C}$ marks the boundary between Unit 3 and Unit 4 (460 cm). Average sedimentary accumulation rate is higher (1.3 mm/yr) in the upper section of Unit 3 and lower (<1 mm/yr) between 380 and 455 cm (Supplementary Data). Higher abundance of *Fragilariopsis kerguelensis*

persists across the transition between Unit 3 and Unit 4 (Fig. 7).

Unit 4a (460–550 cm) is characterized by peak MS, sand abundance, and $\delta^{13}\text{C}$, and relatively low wt% BSi, ADA, TOC, Br/Ti ratio and accumulation rate. Sand abundance, MS, and $\delta^{13}\text{C}$ trend towards lower values between 460 cm and 570 cm while TOC, Br/Ti, and wt% BSi increase. The diatom assemblage is characterized by low relative abundance of *F. curta* and highest relative abundance of *F. obliquecostata* (Fig. 7). Transient elevated wt% BSi and TOC values at 485 and 505 cm correspond to lower MS and sand concentration. Unit 4a (460–550 cm) is distinguished from Unit 4b (550–570 cm) by a trend towards a higher proportion of fine sand, a more coarse-skewed grain size assemblage, higher relative abundance of *T. antarctica*, reduced clay content, and lower sedimentary accumulation (<0.5 mm/yr) (Supplementary Data). Proxy values in Unit 4b resemble those in units 1, 2 and 3.

4. Discussion

Combining a multi-proxy marine sedimentary dataset with modern observations allows us to characterize the Holocene paleoenvironmental history of inner Robertson Bay from the mid-Holocene (6.7 cal kyr BP) to the present (Table 4; Fig. 8; Fig. 9). Instrumental measurements and satellite data provide a snapshot of modern Robertson Bay oceanography (Fig. 2; Fig. 3), which serves as a basis for our interpretation of past changes in primary productivity, sea ice dynamics, polynya activity, and mCDW intrusion within the embayment.

The most prominent feature in the reconstruction is a transition in paleoenvironmental conditions during the mid-to late-Holocene after 4.0 cal kyr BP (3.5–4.7 cal kyr BP, 95% confidence interval). This shift is most evident in proxy indicators for the relative contributions of terrigenous sedimentation (MS) and primary production (wt% BSi, Br/Ti ratio, $\delta^{13}\text{C}$) which dominate the variance in axis 1 of the PCA (Table 1; Fig. 5). Higher values of PCA axis 1 reflect a greater proportion of terrigenous sedimentation whereas lower values indicate greater biogenic flux. The sedimentary accumulation rate also increases from <0.5 mm/yr to >1.0 mm/yr after 4.0 cal yr BP. Transitions ca. 1500 cal

Table 4
Summary of the proxy characteristics and environmental interpretation for each unit.

Unit	Proxy characteristics and environmental interpretation
<i>Little Ice Age</i>	Unit 1a ↑ TOC → preservation of a modern core top
	Unit 1b <0.5 cal kyr BP ↑ ↑ <i>F. curta</i> → onset the modern sea ice cycle (9–11 months of sea ice cover)
	Unit 1c 0.7–01.5 cal kyr BP ↑ δ ¹³ C and ↓ <i>Chaetoceros</i> spp.: CRS ratio → stable, nutrient-limited, surface layer ↑ <i>F. curta</i> → longer duration of sea ice
<i>Early last millennium</i>	Unit 2a 1.0–0.7 cal kyr BP ↓ δ ¹³ C and ↑ <i>Chaetoceros</i> spp.: CRS ratio → mixed, nutrient-rich, surface waters ↑ Mn/Fe ratio → enhanced polynya activity ↑ Sedimentary accumulation → deposition of biogenic and terrigenous sediment
	Unit 2b 1.5–1 cal kyr BP ↑ MS and sand → higher proportion of terrigenous sediment ↓ Wt% BSi, TOC, Br/TI, ADA → reduced primary productivity and export ↓ <i>F. curta</i> → shorter seasonal duration of sea ice
<i>Neoglacial</i>	Unit 3 4.0–1.5 cal kyr BP ↓ δ ¹³ C → nutrient rich, mixed, surface waters ↓ MS and sand % → lower proportion of terrigenous sediment ↑ Wt% BSi, TOC, Br/TI, ADA → primary productivity and export ↑ <i>F. curta</i> → longer seasonal duration of sea ice
<i>Mid-Holocene</i>	Unit 4a 6.2–4.0 cal kyr BP ↓ PCA axis 1 → greater proportion of terrigenous sediment ↓ sedimentary accumulation → reduced primary productivity and export ↑ δ ¹³ C → stratification and primary production within sea ice ↑ <i>F. obliquecostata</i> → year-round sea ice cover ↑ coarse skewed grainsize assemblage → winnowing of sediment by bottom currents
	Unit 4b 6.7–6.2 cal kyr BP Multi-proxy record (PCA axes 1 and 2, grain size assemblage) and individual proxies (e.g. wt% BSi) resemble Unit 3 → seasonally open marine conditions

yr BP and 700 cal yr BP are inferred from shifts in proxies for the seasonal duration of sea ice (*F. curta* relative abundance) and water mass circulation/stratification (Mn/Fe ratio, δ¹³C, and *Chaetoceros* ratio) captured by axis 2 of the PCA. High values of PCA axis 2 are associated with sedimentary proxies for nutrient-rich, mixed surface waters and lower abundance of the diatom *F. curta*, which thrives in melt-stratified conditions at the sea ice edge in regions where seasonal sea-ice duration averages 9–11 months a year (Armand et al., 2005).

4.1. Mid-Holocene [6.7–4.0 cal kyr BP; Unit 4]

We interpret low sediment accumulation (0.4 mm/yr) and proxy indicators of low primary production (TOC, ADA, wt% BSi) during the mid-Holocene as evidence for sedimentary deposition beneath multi-year sea ice or a small ice shelf, particularly after 6.2 cal kyr BP (Fig. 8) (Minzoni et al., 2015; Smith et al., 2019). Sorted, fine sand/coarse silt laminae with coarse-skewed grain size assemblages suggest that moderately strong bottom currents winnowed the seabed or prevented the suspension settling of muds (Supplementary Data; Table 3) (Hemer and Harris, 2003). Highest down-core abundance of *Fragilaria obliquecostata*, characteristic of regions covered year-round by sea ice (Armand et al., 2005; Gersonde and Zielinski, 2000), provides further evidence of ice-capped conditions within the embayment (Fig. 7). Declining biogenic influence and sedimentation rate indicate an increase in the spatial extent of perennial ice cover in inner Robertson Bay between 6.2 cal kyr BP and 4.0 cal kyr BP. We interpret transient increases in biogenic flux approaching late Holocene values as brief recurrences of seasonally open marine conditions associated with ice shelf retreat or the breakup of perennial sea ice.

Relatively higher δ¹³C values (>−24 ‰) from 6.2 to 4.0 cal kyr BP also support the interpretation of either diatom growth within perennial sea ice or increased influence from terrestrial organic matter within an under-ice shelf depositional environment. Changes in the bulk δ¹³C of marine sediment are the result of the interplay between biological productivity, water mass circulation, and terrestrial sources. Primary production enriches the dissolved inorganic carbon pool of surface waters in ¹³C because photosynthesis preferentially removes ¹²C during the production of biomass, which therefore contains a greater proportion ¹²C. Increased biological fractionation will increase the δ¹³C of surface

waters if the carbon pool is not replenished (such as in a semi-stratified sea ice environment) and primary producers record this signature (Geilfus et al., 2015; Gibson et al., 1999; Henley et al., 2012; Tesi et al., 2020). In Antarctic environments, δ¹³C can be interpreted as a proxy for total primary production because the fractionation effect of increased primary production on δ¹³C of surface waters is thought to dominate the effects of oceanographic change (stratification) and species-specific fractionation processes (Berg et al., 2013; Panizzo et al., 2014; Stoll et al., 2017; Villinski et al., 2000). Furthermore, because diatoms thrive in a stratified environment (Leventer and Dunbar, 1996), periods of high primary productivity typically co-occur with increases in stratification, such that both processes operate simultaneously to increase the δ¹³C of surface waters. However, in Robertson Bay, δ¹³C and indicators of primary production (wt% BSi, Br/Ti, TOC) are anticorrelated ($r < -0.80$, $p < 0.001$) and positively correlated with proxies for the relative contribution of terrigenous sediment (MS, sand percentage). This correlation indicates that the combined influence of reduced biogenic flux under nutrient limited, stratified surface conditions (such as within sea ice) and an increase in the relative proportion of terrestrial organic matter exerts primary control on bulk δ¹³C (Fig. 6; Fig. 7; Supplementary Data).

The inferred northward expansion of persistent ice cover in Robertson Bay between 6.2 and 4.0 cal kyr BP coincides with the final phase of glacial and ice sheet retreat in the Ross Embayment between 7 and 3.5 cal kyr BP (Ashley et al., 2021; Jones et al., 2020; Spector et al., 2017) (Fig. 8). This period is also associated with freshened surface waters, inhibited dense water formation, and the absence of CDW on the continental shelf in other regions of the East Antarctic coastal margin (Ashley et al., 2021; Crosta et al., 2018; Denis et al., 2009a; Kim et al., 2012). Based on these observations, we propose that the influence of Antarctic ice sheet in the Ross Embayment and glacial retreat in Robertson Bay during the mid-Holocene may have altered the local oceanographic regime (Ashley et al., 2021), supporting the expansion of multi-year sea ice cover or an expanded ice shelf during the mid-Holocene Hypsithermal climate optimum (Allen et al., 2010; Christ et al., 2015; Crosta et al., 2007; Kim et al., 2018; Leventer et al., 1996; Minzoni et al., 2015; Panizzo et al., 2014; Peck et al., 2015; Pike et al., 2009; Totten et al., 2022).

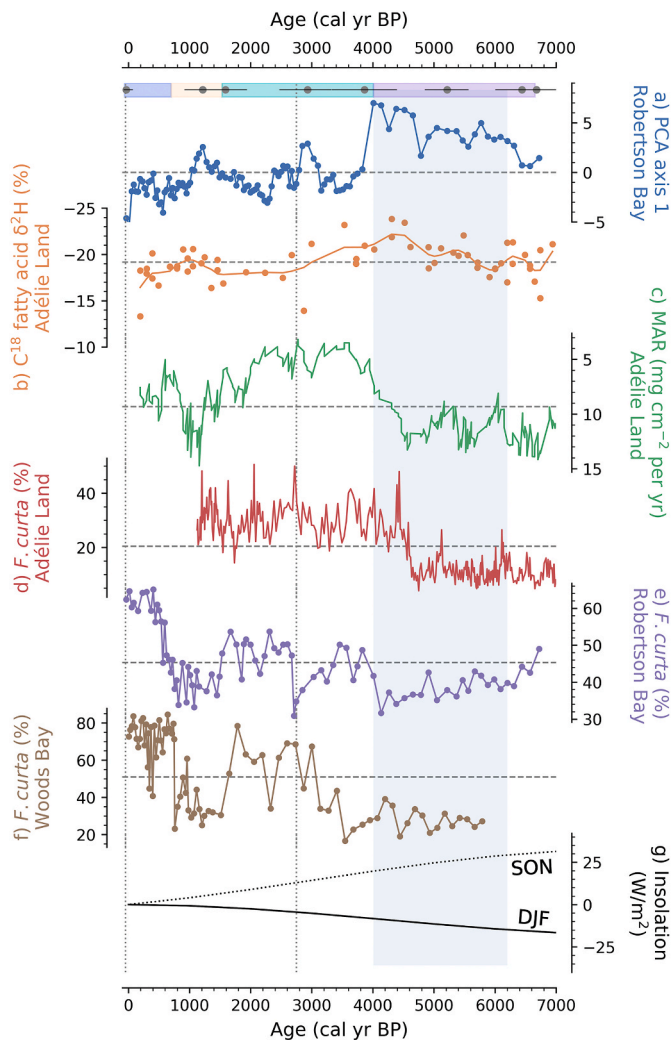


Fig. 8. Millennial-scale Holocene variability. Top circles show dated horizons in core RS15-GC57. Colored bars indicate the sedimentary units discussed in text (Unit 1 = blue; Unit 2 = beige; Unit 3 = teal; Unit 4 = purple). Dashed line indicates the Holocene average for the record. Inferred ice-capped conditions in inner Robertson Bay highlighted by the shaded blue bar between 6200 and 4000 cal yr BP; (a) PCA axis 1 (this study); (b) $\delta^2\text{H}$ C^{18} fatty acid with locally weighted smoothing at Site U1357 in Adélie Land, East Antarctica (Ashley et al., 2021); (c) mass accumulation rates of biogenic material at Site U1357 in Adélie Land (Ashley et al., 2021); (d) relative abundance of *F. curta* from core MD03-2601 interpreted as a proxy for sea ice extent and duration in Adélie Land (Crosta et al., 2008; age model adapted in Ashley et al., 2021); (e) *F. curta* relative abundance from Robertson Bay (this study); (f) Relative abundance of *F. curta* from core WRS_WB interpreted as a proxy for sea ice extent and duration in the northwest Ross Sea (Mezgec et al., 2017). (g) insolation anomaly from 2000 CE at 71°S for September, October, and November (SON) and December, January, and February (DJF) (Laskar et al., 2004). Dotted lines show time period highlighted in Fig. 9.

4.2. Onset of the Neoglacial [ca. 4.0 cal kyr BP, Unit 3–4 transition]

A step-change in TOC, wt% BSi, and MS values and sedimentation rate ca. 4.0 cal kyr BP is consistent with the establishment of seasonally open marine conditions in Robertson Bay (Smith et al., 2019). After 4.0 cal kyr BP, $\delta^{13}\text{C}$ values of less than -24% are within the range of modern values for seasonally open marine conditions in Robertson Bay and other regions of the Ross Sea (Villinski et al., 2000). Higher abundances of *F. kerguelensis*, a diatom species associated with SSTs $>1^\circ\text{C}$ (Armand et al., 2005; Crosta et al., 2005) occur during the inferred breakup of ice-covered conditions ca. 4.0 cal kyr BP, indicating that

warmer ocean temperatures may have played a role in establishing open water conditions within the inner basin of Robertson Bay.

The curvate and blocky nature of deformation in the laminated sandy muds persists in core RS15-GC57 from the base of the core at 6.7 cal kyr BP until ca. 3.2 cal kyr BP (2.7–3.7 cal kyr BP, 95% CI), consistent with the ongoing influence of local ice-shelf breakup after open-water conditions were established over the core site. In contrast, such deformation is absent after 3.2 cal kyr BP, suggesting that deep-draft icebergs occupied Robertson Bay after open marine conditions were established over the core site ca. 4.0 cal kyr BP but were absent during the late Holocene. Enhanced discharge of icebergs derived from thickened ice sheets that were previously buttressed by an ice shelf or multi-year fast ice would be anticipated following the collapse of the ice shelf (Wise et al., 2017). Iceberg keel depth would also reduce after thinning of the inland ice sheet had occurred, explaining a lack of scouring after 3.2 cal kyr BP.

Oceanographic feedbacks linked to the stabilization of the Antarctic ice sheets in the Ross Embayment and outlet glaciers along the Victoria Land coast provide a potential mechanism for the onset of seasonally open marine conditions and higher rates of primary production in Robertson Bay ca. 4.0 cal kyr BP (cf. Ashley et al., 2021). This transition occurs against the backdrop of more gradual trends in seasonal insolation (Fig. 8). Colder temperatures during summer and autumn linked to changes in seasonal insolation south of 60°S may have also supported more consolidated, multi-year sea ice or an expanded ice shelf in Robertson Bay during the mid-Holocene (cf. Crosta et al., 2018; Pike et al., 2009). However, the inferred expansion of multi-year ice cover after 6.2 cal kyr BP and break-up ca. 4.0 cal kyr BP is inconsistent with a monotonic trend in seasonal insolation during the late Holocene (Fig. 8). Additionally, evidence of ice covered conditions in Robertson Bay is at odds with marine records of an Antarctic mid-Holocene Hypsithermal climatic optimum characterized by higher rates of primary productivity, warmer conditions in spring and early summer, and a longer ice free season along the Adélie land margin and the Antarctic Peninsula relative to the late Holocene (Allen et al., 2010; Christ et al., 2015; Crosta et al., 2007; Kim et al., 2018; Leventer et al., 1996; Minzoni et al., 2015; Panizzo et al., 2014; Peck et al., 2015; Pike et al., 2009; Totten et al., 2022). We invoke local influence and feedbacks relating to glacier and ice sheet retreat and meltwater discharge as a mechanism to reconcile our inference of persistent ice cover in Robertson Bay between 6.2 and 4.0 cal kyr BP and low sedimentation rates and other coastal western Ross Sea sediment cores (Mezgec et al., 2017) with marine records of a mid-Holocene climatic optimum in other regions.

Marine sediment cores from both the Antarctic Peninsula and East Antarctic margin also show a base-line shift in coastal sea ice between 4.5 and 2.5 cal kyr BP, which characterizes the transition from the mid-Holocene conditions to colder, more variable, late Holocene Neoglacial conditions (Ashley et al., 2021; Domack et al., 2001; Johnson et al., 2021; Peck et al., 2015; Totten et al., 2022). Following Ashley et al. (2021), we emphasize the potential influence of regionally specific ice-ocean feedbacks in driving this transition, which is characterized by the inferred breakup of perennial ice cover in Robertson Bay and an increase in the seasonal duration of sea ice in other regions of the Antarctic margin (Crosta et al., 2007; Taylor et al., 2001; Totten et al., 2022). The mid-to-late Holocene transition occurs ~ 1000 years earlier in Antarctic marine records from the Ross Sea and Adélie Land (ca. 3.5–4.5 kyr BP) than the Antarctic Peninsula (ca. 2.5–3.5 kyr BP) (Bentley et al., 2009; Johnson et al., 2021; Mezgec et al., 2017; Totten et al., 2022). This discrepancy may be related to the timing of ice sheet retreat and differing oceanographic regimes and ice-ocean feedbacks in East and West Antarctica.

4.3. Late Holocene Neoglacial [4.0–1.5 cal kyr BP, Unit 3]

Following the establishment of open-marine conditions in Robertson Bay ca. 4.0 kyr BP, the relative abundance of the diatom *F. curta* can be used to infer changes in the seasonal duration of sea ice (Armand et al.,

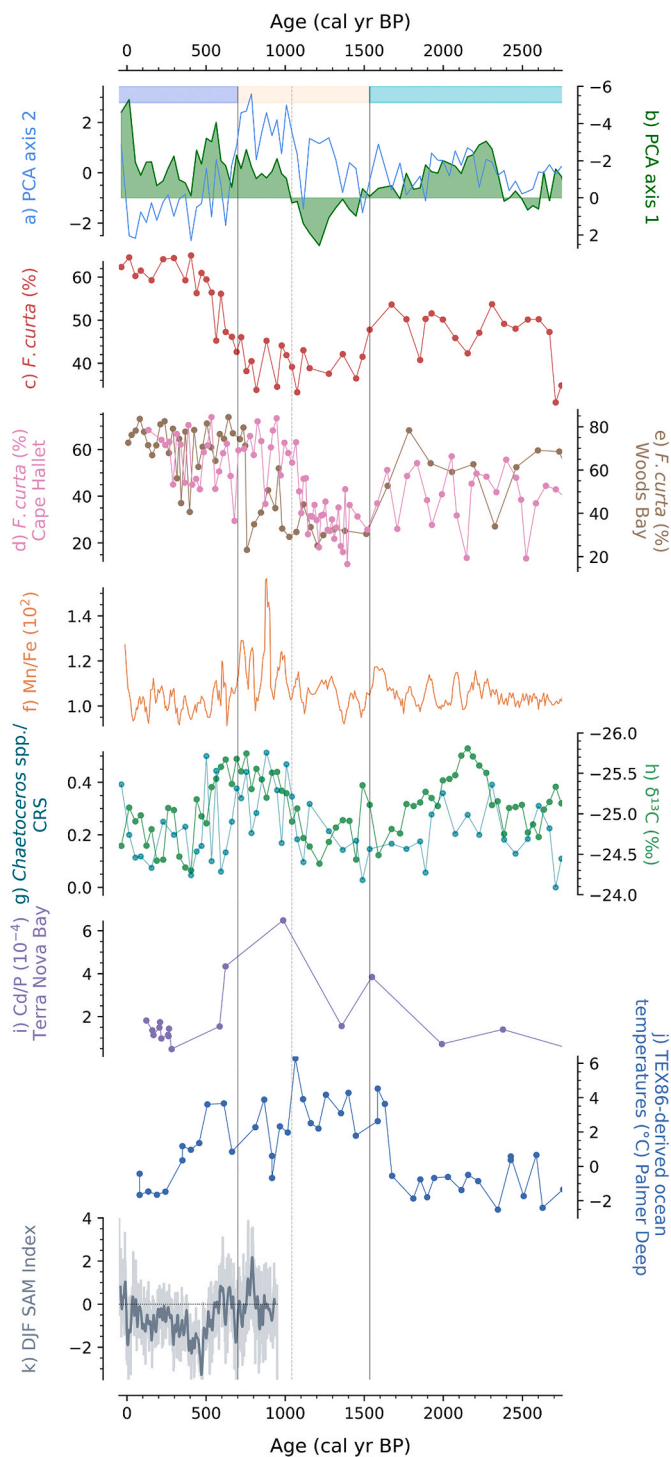


Fig. 9. Climate evolution during the late Holocene. Colored bars highlight the sedimentary units discussed in text (Unit 1 = blue; Unit 2 = beige; Unit 3 = teal). Dashed line shows Unit 2a and Unit 2b boundary. (a) PCA axis 1 (this study); (b) PCA axis 2 (this study); (c) *F. curta* relative abundance (this study); (d) *F. curta* relative abundance near Cape Hallett (Mezgec et al., 2017); (e) *F. curta* relative abundance near Woods Bay (Mezgec et al., 2017); (f) Mn/Fe ratio (this study); (g) *Chaetoceros* spp./CRS ratio (this study); (h) $\delta^{13}\text{C}$ in Robertson Bay (this study); (i) Cd/P ratio in Terra Nova Bay, interpreted as increased nutrient supply and CDW upwelling (Xu et al., 2021); (j) TEX86 derived ocean temperatures in the Palmer Deep, Antarctic Peninsula (Shevenell et al., 2011); and (k) reconstructed summer (DJF) SAM Index with 30-yr loess smoothing (dark grey), horizontal line shows average across the record (Dätwyler et al., 2018).

2005). Higher abundances of *F. curta* in Robertson Bay and farther south in Cape Hallett and Woods Bay (Mezgec et al., 2017) during the late Holocene are characteristic of a similar-to-modern duration of the summer open water season (1–3 months) and persistent sea ice meltwater stratification in spring (Fig. 8). *Fragilariopsis curta* is seeded by melting pack/fast ice and dominates the meltwater-stratified ice edge of the Ross Sea during the austral spring and early summer (Cunningham and Leventer, 1998). The relative abundance of *F. curta* in core RS15-GC57 is negatively correlated with indicators of a more nutrient rich, mixed surface layer (*Chaetoceros* ratio) and oxygenated conditions in the deep basin of Robertson Bay (Mn/Fe), which we interpret as a signature of enhanced polynya activity (Table 1; Fig. 5). This inverse relationship, represented by axis 2 of the PCA, aligns with *F. curta*'s preference for the spring sea ice meltwater-stratified environment, which is sustained by northerly winds along the East Antarctic margin (Campagne et al., 2016; Leventer and Dunbar, 1996). However, we also note the significant influence of seasonality on these proxies; *F. curta* is primarily associated with spring sea ice conditions, whereas open polynya conditions in Robertson Bay occur in April (austral autumn) during the satellite period (Fig. 3).

Fragilariopsis curta relative abundance is generally higher between 4.0 cal kyr BP and 1.5 cal kyr BP (40–50%). A transient decrease to 35% is consistent with a short term (~500 year) reestablishment of multi-year ice cover ca. 2.9 cal kyr BP (2.5–3.3 cal kyr BP, 95% CI) (Fig. 9). This interpretation is supported by grainsize analysis, which is also more characteristic of mid-Holocene conditions (Supplementary Data) and a decline in biogenic sedimentation (Fig. 9). The spike in CRS relative abundance following this interval may be associated with meltwater stratification in the surface layer following perennial ice breakup (e.g. Hillenbrand et al., 2010), possibly due to the influence of warmer ocean temperatures.

4.4. Last millennium environmental variability [1.5–0.7 cal kyr BP, Unit 2]

Fluctuations in *F. curta* abundance and proxies for biogenic sedimentation in Robertson Bay and along the Victoria Land margin indicate shifts in sea ice dynamics and nutrient availability during the period between 1.5 and 0.7 cal kyr BP (Mezgec et al., 2017). Lower *F. curta* abundance in Robertson Bay (<40%) is characteristic of a reduction in spring sea ice concentration and a longer summer open water season (Armand et al., 2005). Reduced spring sea ice concentrations in Robertson Bay between 1.5 and 0.7 cal kyr BP is broadly consistent with regional records from the Victoria Land coastal margin (Mezgec et al., 2017; Tesi et al., 2020). A longer open-water season in the embayment may have supported the expansion of the Cape Adare Adélie penguin colony, which reached its maximum size ca. 1.2 cal kyr BP (Emslie et al., 2018). Marine records located farther south along the Victoria Land coast (Mezgec et al., 2017) and Adélie Land (Johnson et al., 2021), are also consistent with a decrease in coastal sea ice after 1.5 cal kyr BP. Proxies for biogenic sedimentation (axis 1 of the PCA) indicate reduced primary production in Robertson Bay until 1.0 cal kyr BP despite a longer ice free season (Table 4; Fig. 9), perhaps due to nutrient limitation within the surface layer. A greater relative abundance of CRS relative to *Chaetoceros* spp. supports the interpretation of reduced primary productivity under nutrient-limited conditions because *Chaetoceros* spp. form resting spores under nutrient-depleted conditions (Leventer et al., 1996).

Our interpretation of nutrient-limited conditions in Robertson Bay during the period from 1.5 cal kyr BP to 1.0 cal kyr BP contrasts with evidence of intensified upwelling of nutrient-rich mCDW and enhanced productivity along both the East and West Antarctic margins (Fig. 7; Fig. 8) (Johnson et al., 2021; Kim et al., 2012; Shevenell et al., 2011). This offset may be an artifact of radiocarbon dating uncertainty, which is greater than 300 years in the upper section of our reconstruction. However, we also note that this discrepancy is consistent with the

oceanographic regime along the Victoria Land coastal margin. In the modern environment, brine rejection during sea ice production in autumn breaks down the salinity gradient in the water column, oxygenating the inner basin of Robertson Bay and driving cross-shelf exchange of warmer, nutrient rich, waters, present off the shelf at Cape Adare (Gordon et al., 2015) (Fig. 3). We hypothesize that a longer and warmer summer season inferred from terrestrial records ca 1.4 cal kyr BP (Jin et al., 2021; Mezgec et al., 2017; Stenni et al., 2017) may have restricted polynya formation in Robertson Bay and other regions of the Victoria Land coastal margin, thereby reducing associated transport of nutrient rich CDW into the surface layer (Mezgec et al., 2017; Morrison et al., 2020; Xu et al., 2021). The breakdown of spring meltwater stratification and a destabilized water column, which transports diatoms below the pycnocline (Höfer et al., 2019), could have further acted to limit primary production in Robertson Bay during a period of reduced spring sea ice concentrations.

A higher ratio of *Chaetoceros* spp. to CRS and more negative $\delta^{13}\text{C}$ during the early part of the last millennium (ca. 0.8 cal kyr BP) is consistent with a period of more nutrient-rich, mixed surface waters in Robertson Bay, which supported increased biogenic flux (Fig. 9). Peak Mn/Fe ratio indicates a period of more oxygen-rich conditions in the deep basin of Robertson Bay. Taken together, we interpret the proxy records to indicate active polynya formation and production of denser-than-modern waters within the embayment. In the modern environment, the cold, oxygenated water mass produced in Robertson Bay's autumn polynya is displaced by warmer, less oxygenated mCDW (Fig. 3). We propose that enhanced polynya efficiency ca. 0.8 cal kyr BP could have produced a cold and oxygenated water mass of sufficient density to displace the warmer, saltier, less oxygenated water mass which occupies the deep basin in the modern day (Fig. 2; Fig. 3), while outflow of dense waters drove enhanced compensatory inflow of CDW into the embayment at intermediate depths.

Nutrient-replete conditions in the surface layer of Robertson Bay ca. 0.8 cal kyr BP are consistent with an increase in nutrient availability further south in the Terra Nova Bay region, which has been linked to greater on-shelf presence of mCDW between 1.0 and 0.6 cal kyr BP (Fig. 9) (Xu et al., 2021). The delayed onset of peak mCDW influence and primary productivity in the Ross Sea relative to the Antarctic Peninsula, where warmer subsurface temperatures are observed after 1.6 cal kyr BP (Shevenell et al., 2011), is consistent with the differing oceanographic regimes. Modified Circumpolar Deep Water flows directly onto the shelf on the Antarctic Peninsula (Thompson et al., 2018). By contrast, mCDW intrusion into Robertson Bay and the wider Ross Sea region is modulated by dense water production and export (Morrison et al., 2020; Thompson et al., 2018) and may have been inhibited by warmer climate conditions and suppressed polynya along the Victoria Land Coast before 1.0 cal kyr BP (An et al., 2021; Mezgec et al., 2017).

Our interpretation of enhanced polynya activity in Robertson Bay ca. 0.8 cal kyr BP is broadly consistent with previous research which identifies mean state changes in the Southern Annular Mode (SAM) and the El Niño/Southern Oscillation (ENSO) as a dominant control on last millennium Ross Sea climate (Bertler et al., 2018; Koffman et al., 2023; Lüning et al., 2019). Increased upwelling of CDW along the margin the Antarctic Peninsula (Shevenell et al., 2011) and a strengthening of atmospheric circulation along the Siple Coast (Koffman et al., 2023) has been linked to intensified Southern Hemisphere Westerly Winds associated with a multi-centennial trend towards a positive phase of the SAM during the early part of the last millennium (Dätwyler et al., 2018; Goodwin et al., 2014; Hinojosa et al., 2017; Koffman et al., 2014; Perren et al., 2020). A sustained positive phase of the SAM and an increased prevalence of the La Niña phase of ENSO ca. 0.8 cal kyr BP (Goodwin et al., 2014; Hinojosa et al., 2017) may have acted to enhance southerly and katabatic winds in the coastal Ross Sea (Stammerjohn et al., 2008). Stronger southerly winds promote dense water production, compensatory inflow of mCDW, and earlier sea ice breakout during the summer ice-free season in the Ross Sea (Morrison et al., 2020; Schine et al., 2016).

Considered together, Ross Sea paleoclimate records are consistent with a role for large scale modes of climate variability in driving an increase in CDW upwelling, primary productivity, and polynya activity along the Victoria Land margin during the first part of the last millennium (ca. 0.8 cal kyr BP), a period that has been characterized as Antarctic manifestation of the MCA (Lüning et al., 2019 and references therein). However, we note that evidence of baseline shifts in SAM and ENSO dynamics during the early part of the last millennium remain equivocal (Henke et al., 2017; King et al., 2023), and further work is required to conclusively link late Holocene Antarctic climate evolution to multi-centennial trends in dynamic modes of climate variability (Johnson et al., 2021; Truax et al., 2022).

4.5. Little Ice Age [0.7 cal kyr BP – present; Unit 1]

Reconstructions from Robertson Bay and other coastal sediment cores from the western Ross Sea indicate an increase in the seasonal duration of sea ice between 0.7 cal kyr BP and the present, consistent with ice core temperature reconstructions of cooling atmospheric temperatures (Fig. 9) (Bertler et al., 2011; Orsi et al., 2012; Rhodes et al., 2012; Stenni et al., 2017; Tesi et al., 2020). This shift towards more consolidated last millennium sea ice conditions in the Cape Hallett region, located less than 100 km south of Robertson Bay, has been dated to ca. 0.7 cal kyr BP using tephrochronology (Di Roberto et al., 2019; Mezgec et al., 2017; Tesi et al., 2020). The onset of icier spring conditions in Robertson Bay, inferred from the relative abundances of *F. curta* and *T. antarctica* also occurs at 0.7 cal kyr BP, which provides confidence in the accuracy of the core's radiocarbon-based chronology. We interpret a lower Mn/Fe ratio after 0.7 cal kyr BP as a decrease in bottom water oxygenation within the inner basin of Robertson Bay (Fig. 9). Proxies for nutrient-rich, mixed surface waters (*Chaetoceros* ratio and $\delta^{13}\text{C}$) decline after 0.7 cal kyr BP, consistent with a reduction in nutrient-rich mCDW in the upper water column (cf. Xu et al., 2021). Indicators of primary productivity in Robertson Bay (axis 2 of the PCA) remained elevated relative to the Holocene baseline, perhaps due to alternative sources of nutrients such as iron fertilization from dust sourced from the nearby McMurdo Volcanic Group (Kyle, 1990; Winton et al., 2014) and favorable conditions for diatom growth in a sea ice meltwater-stratified surface layer (Leventer and Dunbar, 1996).

Icier spring conditions and a sea-ice meltwater stratified surface layer in Robertson Bay, particularly after 0.5 cal kyr BP, are consistent with marine and terrestrial records of an Antarctic Little Ice Age (LIA) (Orsi et al., 2012; Rhodes et al., 2012; Simms et al., 2021; Totten et al., 2022). The interplay between an externally forced last millennium cooling trend (Neukom et al., 2019; Otto-Bliesner et al., 2015; Truax et al., 2022) and a multi-centennial shift towards the negative phase of the SAM after 0.6 cal kyr BP (Abram et al., 2014; Dätwyler et al., 2018; Goodwin et al., 2014; Perren et al., 2020) could have supported more consolidated sea ice conditions in the western Ross Sea. However, the increase in spring sea ice concentrations persisted along the Victoria Land coastal margin after the mean state of the SAM became more positive ca. 0.3 cal kyr BP (Abram et al., 2014; Dätwyler et al., 2018; Sadai et al., 2020), which suggests that atmospheric cooling over the Victoria Land region may have exerted primary control over sea ice conditions in the Ross Sea during the LIA (Mezgec et al., 2017; Rhodes et al., 2012; Stenni et al., 2017; Tesi et al., 2020). We speculate that the persistence of consolidated coastal sea ice conditions along the Victoria Land coastal margin to the present day (Tesi et al., 2020), despite warming atmospheric temperatures after 1850 CE (Rhodes et al., 2012; Stenni et al., 2017), and a positive trend in the SAM since 1950 CE (Marshall, 2003), may be associated with the modern influence of West Antarctic Ice Sheet melt. Increasing mass loss from the WAIS has freshened surface waters in the Ross Sea since the 1950s (Jacobs et al., 2022), and freshened surface waters could support more consolidated sea ice conditions despite atmospheric forcing (e.g. Bintanja et al., 2013).

5. Conclusions

Our multi-proxy record of changing ocean conditions at the intersection between the Ross Sea and the Southern Ocean provides new perspective on the influence of ice sheet and glacial retreat on mid-Holocene oceanographic conditions. We interpret indicators of persistent ice cover in Robertson Bay between 6.2 and 4.0 cal kyr BP as a local response to AIS retreat during the mid-Holocene. We propose that meltwater discharge associated with the formation of the modern Ross Ice Shelf and glacial retreat along the Victoria Land coastal margin altered the structure of the continental shelf-break frontal system, freshening surface waters and isolating downstream regions of the East Antarctic margin from upwelling mCDW. Both regional processes and the local retreat of glaciers within the embayment could have supported the expansion of multi-year sea ice or a small-cavity ice shelf in inner Robertson Bay during a period characterized by warmer spring conditions and increased primary production in other regions of Antarctica. We suggest that ice sheet retreat was an important, perhaps dominant, driver of contrasting mid-Holocene environmental conditions around the Antarctic margin. The formation of modern ice shelf cavities and the onset of modern-style water mass transformation is a plausible mechanism for rapid environmental change against the backdrop of more gradual trends in seasonal insolation (cf. [Ashley et al., 2021](#)). This result underscores that the mid-to-late Holocene transition, recorded in Antarctic marine sediment cores (ca. 4 cal kyr BP), is a valuable target for coupled ice sheet-ocean modeling studies which seek to understand the regional impact of Antarctic ice sheet retreat and the ice-ocean feedbacks that support ice sheet readvance (cf. [Venturelli et al., 2020](#)).

Greater influence of global modes of atmospheric variability and climate evolution (SAM, ENSO, insolation changes, volcanic eruptions) on late Holocene Ross Sea oceanography is consistent with the termination of regional forcing associated with Antarctic ice sheet retreat. Variability in *F. curta* relative abundance and other indicators of sea ice and oceanographic dynamics in Robertson Bay and other regions of the Victoria Land coastal margin indicate relatively large environmental shifts during the late Holocene, despite subtle changes in external forcings. We identify a period associated with a shorter seasonal duration of sea ice, reduced polynya activity, and nutrient limitation in Robertson Bay between 1.5 and 1.0 cal kyr BP. A subsequent increase in productivity and bottom water oxygenation ca. 0.8 cal kyr BP is consistent with enhanced polynya activity, a greater presence of mCDW in the surface layer, and displacement of oxygen-poor mCDW from the deep basin of Robertson Bay. These conditions coincide with the core period of an Antarctic MCA. After 0.7 cal kyr BP, more consolidated sea ice conditions in Robertson Bay persist during the Little Ice Age, a period of colder atmospheric temperatures in Ross Sea linked to orbital, volcanic and solar forcing, and a sustained negative trend in the SAM. In contrast to the mid-to-late Holocene, last millennium climate transitions were more regionally consistent, and the Little Ice Age recorded in terrestrial and marine records from West and East Antarctica (onset 700–400 cal yr BP) is more synchronous than any prior event.

Holocene marine paleoclimate records from Robertson Bay and across the Antarctic margin record the oceanographic response to mid-Holocene glacial retreat, as well as natural variability in SAM and ENSO dynamics and global mean temperatures during the last millennium. These findings highlight the likely sensitivity of the Antarctic ice-ocean interface to projected changes in AIS meltwater discharge, global mean temperatures, SAM, and ENSO in the coming decades. Furthermore, the regionally specific impact of mid-Holocene ice sheet retreat underlines the critical need to integrate and accurately represent feedback mechanisms between Antarctic oceanography and ice sheet dynamics in projections of future changes.

Credit author statement

OJT: Conceptualization, Formal analysis, Investigation; Data curation, Visualization, Writing – original draft, Writing – review & editing; **CRR:** Conceptualization, Investigation, Methodology, Validation; Resources, Writing – review & editing; Supervision; Project administration; Funding acquisition; **GSW:** Conceptualization, Resources, Writing – review & editing; Supervision, Project administration; Funding acquisition; **CS:** Conceptualization, Writing – review & editing; Supervision, Funding acquisition; **RLP:** Investigation, Data curation, Writing – review & editing; **JIL:** Conceptualization, Investigation, Resources, Writing – review & editing; Funding acquisition; **RM:** Formal analysis, Writing – review & editing; Funding acquisition; **BR:** Methodology, Formal analysis, Validation, Writing – review & editing; **CEG:** Investigation, Methodology, Formal analysis, Validation, Writing – review & editing; **JCT:** Investigation, Methodology, Formal analysis, Validation, Writing – review & editing; Funding acquisition; **HSM:** Investigation; **MKL:** Conceptualization, Investigation, Funding acquisition; **BD:** Investigation; **KCY:** Conceptualization, Investigation, Funding acquisition.

Declaration of competing interest

The authors declare that they have no known competing financial interests or personal relationships that could have appeared to influence the work reported in this paper.

Data availability

The new multi-proxy data from core RS15-GC57 and instrumental measurements from Robertson Bay presented in this paper are available in the [Supplementary Data](#).

Acknowledgements

We gratefully acknowledge the science party, technicians, and crew of R/V *Araon* expedition ANA05B for facilitating the data collection, sediment coring and mooring deployments that provide the foundation for this work. Fieldwork at Cape Adare was supported by the New Zealand Antarctic Research Institute, and we thank Craig Cary for assistance with weather station data collection. Sincere thanks to Richard Levy, Environment and Climate Theme Leader at GNS Science, for his support and leadership in establishing the collaboration that facilitated the fieldwork and subsequent research. This work was funded by the Korea Polar Research Institute (project PE24090 funded by the Ministry of Oceans and Fisheries), the New Zealand Ministry of Business, Innovation and Employment (MBIE) Past Antarctic Climate and Future Implications Programme (contract C05X1001), and the MBIE Antarctic Science Platform (contract ANTA1801), with additional support to CRR from a University of Otago Research Grant and a L'Oréal-UNESCO For Women in Science Australia and New Zealand Fellowship. OJT gratefully acknowledges additional funding from Fulbright New Zealand, Antarctica New Zealand, Amherst College, and the University of Otago. The authors acknowledge the use of imagery from the NASA Worldview application (<https://worldview.earthdata.nasa.gov/>), part of the NASA Earth Observing System Data and Information System. RPO-AMS and Py-GC-MS techniques was funded by the New Zealand Ministry of Business, Innovation and Employment (MBIE) through the Global Change Through Time research program (contract C05X1702). Thank you to the Rafter Radiocarbon Laboratory team for radiocarbon sample processing and measurement. We thank Chris Moy for advice on the interpretation of XRF measurements, and David Mucciarone, Fiona Elliott, Hamish Bowman, Gemma Kerr, and Faye Nelson for technical support.

Appendix A. Supplementary data

Supplementary data to this article can be found online at <https://doi.org/10.1016/j.quascirev.2024.108635>.

References

- Abram, N.J., Mulvaney, R., Vimeux, F., Phipps, S.J., Turner, J., England, M.H., 2014. Evolution of the Southern Annular Mode during the past millennium. *Nat. Clim. Change* 4, 564–569. <https://doi.org/10.1038/nclimate2235>.
- Adhikari, P.L., Maiti, K., Overton, E.B., Rosenheim, B.E., Marx, B.D., 2016. Distributions and accumulation rates of polycyclic aromatic hydrocarbons in the northern Gulf of Mexico sediments. *Environ. Pollut. Barking Essex* 212 (1987), 413–423. <https://doi.org/10.1016/j.envpol.2016.01.064>.
- Agnihotri, R., Altabet, M.A., Herbert, T.D., Tierney, J.E., 2008. Subdecadal resolved paleoceanography of the Peru margin during the last two millennia. *Geochem. Geophys. Geosystems* 9. <https://doi.org/10.1029/2007GC001744>.
- Allen, C.S., Oakes-Fretwell, L., Anderson, J.B., Hodgson, D.A., 2010. A record of Holocene glacial and oceanographic variability in Neny Fjord, Antarctic Peninsula. *Holocene* 20, 551–564. <https://doi.org/10.1177/0959683609356581>.
- An, C., Hou, S., Jiang, S., Li, Y., Ma, T., Curran, M.A.J., Pang, H., Zhang, Z., Zhang, W., Yu, J., Liu, K., Shi, G., Ma, H., Sun, B., 2021. The Long-Term Cooling Trend in East Antarctic Plateau Over the Past 2000 Years Is Only Robust Between 550 and 1550 CE. *Geophys. Res. Lett.* 48, e2021GL092923 <https://doi.org/10.1029/2021GL092923>.
- Armand, L.K., Crosta, X., Romero, O., Pichon, J.-J., 2005. The biogeography of major diatom taxa in Southern Ocean sediments: 1. Sea ice related species. *Palaeogeogr. Palaeoclimatol. Palaeoecol.* 223, 93–126. <https://doi.org/10.1016/j.palaeo.2005.02.015>.
- Ashley, K.E., McKay, R., Etourneau, J., Jimenez-Espejo, F.J., Condron, A., Albot, A., Crosta, X., Riesselman, C., Seki, O., Massé, G., Golledge, N.R., Gasson, E., Lowry, D.P., Barrand, N.E., Johnson, K., Bertler, N., Escutia, C., Dunbar, R., Bendle, J.A., 2021. Mid-Holocene Antarctic sea-ice increase driven by marine ice sheet retreat. *Climate of the Past* 17, 1–19. <https://doi.org/10.5194/cp-17-1-2021>.
- Beans, C., Hecq, J.H., Koubbi, P., Vallet, C., Wright, S., Goffart, A., 2008. A study of the diatom-dominated microplankton summer assemblages in coastal waters from Terre Adélie to the Mertz Glacier, East Antarctica (139°E–145°E). *Polar Biol.* 31, 1101–1117. <https://doi.org/10.1007/s00300-008-0452-x>.
- Bentley, M.J., Hodgson, D.A., Smith, J.A., Cofaigh, C. ó, Domack, E.W., Larter, R.D., Roberts, S.J., Brachfeld, S., Leventer, A., Hjort, C., Hillenbrand, C.-D., Evans, J., 2009. Mechanisms of Holocene palaeoenvironmental change in the Antarctic Peninsula region. *Holocene* 19, 51–69. <https://doi.org/10.1177/0959683608096603>.
- Berg, S., Leng, M.J., Kendrick, C.P., Cremer, H., Wagner, B., 2013. Bulk sediment and diatom silica carbon isotope composition from coastal marine sediments off East Antarctica. *Silicon* 5, 19–34. <https://doi.org/10.1007/s12633-012-9113-3>.
- Bertler, N.A.N., Conway, H., Dahl-Jensen, D., Emanuelson, D.B., Winstrup, M., Vallelonga, P.T., Lee, J.E., Brook, E.J., Severinghaus, J.P., Fudge, T.J., Keller, E.D., Baisden, W.T., Hindmarsh, R.C.A., Neff, P.D., Blunier, T., Edwards, R., Mayewski, P.A., Kipfstuhl, S., Buizert, C., Canessa, S., Dacic, R., Kjær, H.A., Kurbatov, A., Zhang, D., Waddington, E.D., Baccolo, G., Beers, T., Brightley, H.J., Carter, L., Clemens-Sewall, D., Ciobanu, V.G., Delmonte, B., Eling, L., Ellis, A., Ganesh, S., Golledge, N.R., Haines, S., Handley, M., Hawley, R.L., Hogan, C.M., Johnson, K.M., Korotkiikh, E., Lowry, D.P., Mandeno, D., McKay, R.M., Menking, J.A., Naish, T.R., Noerling, C., Ollive, A., Orsi, A., Proemse, B.C., Pyne, A.R., Pyne, R.L., Renwick, J., Scherer, R.P., Semper, S., Simonsen, M., Sneed, S.B., Steig, E.J., Tuohy, A., Venugopal, A.U., Valero-Delgado, F., Venkatesh, J., Wang, F., Wang, S., Winski, D.A., Winton, V.H.L., Whiteford, A., Xiao, C., Yang, J., Zhang, X., 2018. The Ross Sea Dipole – temperature, snow accumulation and sea ice variability in the Ross Sea region, Antarctica, over the past 2700 years. *Clim. Past* 14, 193–214. <https://doi.org/10.5194/cp-14-193-2018>.
- Bertler, N.A.N., Mayewski, P.A., Carter, L., 2011. Cold conditions in Antarctica during the Little Ice Age – implications for abrupt climate change mechanisms. *Earth Planet. Sci. Lett.* 308, 41–51. <https://doi.org/10.1016/j.epsl.2011.05.021>.
- Bianchi, T.S., Galy, V., Rosenheim, B.E., Shields, M., Cui, X., Van Metre, P., 2015. Paleoreconstruction of organic carbon inputs to an oxbow lake in the Mississippi River watershed: effects of dam construction and land use change on regional inputs. *Geophys. Res. Lett.* 42, 7983–7991. <https://doi.org/10.1002/2015GL065595>.
- Bintanja, R., Van Oldenborgh, G.J., Drijfhout, S.S., Wouters, B., Katsman, C.A., 2013. Important role for ocean warming and increased ice-shelf melt in Antarctic sea-ice expansion. *Nature Geosci* 6, 376–379. <https://doi.org/10.1038/ngeo1767>.
- Bowen, M.M., Fernandez, D., Forcen-Vazquez, A., Gordon, A.L., Huber, B., Castagno, P., Falco, P., 2021. The role of tides in bottom water export from the western Ross Sea. *Sci. Rep.* 11, 2246. <https://doi.org/10.1038/s41598-021-81793-5>.
- Brachfeld, S.A., Banerjee, S.K., 2000. Rock-magnetic carriers of century-scale susceptibility cycles in glacial-marine sediments from the Palmer Deep, Antarctic Peninsula. *Earth Planet. Sci. Lett.* 176, 443–455. [https://doi.org/10.1016/S0012-821X\(00\)00008-X](https://doi.org/10.1016/S0012-821X(00)00008-X).
- Bronsele, B., Winton, M., Griffies, S.M., Hurlin, W.J., Rodgers, K.B., Sergienko, O.V., Stouffer, R.J., Russell, J.L., 2018. Change in future climate due to Antarctic meltwater. *Nature*. <https://doi.org/10.1038/s41586-018-0712-z>.
- Campagne, P., Crosta, X., Schmidt, S., Noëlle Houssais, M., Ther, O., Massé, G., 2016. Sedimentary response to sea ice and atmospheric variability over the instrumental period off Adélie Land, East Antarctica. *Biogeosciences* 13, 4205–4218. <https://doi.org/10.5194/bg-13-4205-2016>.
- Christ, A.J., Talaia-Murray, M., Elking, N., Domack, E.W., Leventer, A., Lavoie, C., Brachfeld, S., Yoo, K.-C., Gilbert, R., Jeong, S.-M., Petrushak, S., Wellner, J., the LARISSA Group, 2015. Late Holocene glacial advance and ice shelf growth in Barilari Bay, Graham Land, West Antarctic Peninsula. *Geol. Soc. Am. Bull.* 127, 297–315. <https://doi.org/10.1130/B31035.1>.
- Crosta, X., Crespin, J., Swingedouw, D., Marti, O., Masson-Delmotte, V., Etourneau, J., Goosse, H., Braconnot, P., Yam, R., Brailovski, I., Shemesh, A., 2018. Ocean as the main driver of Antarctic ice sheet retreat during the Holocene. *Glob. Planet. Change* 166, 62–74. <https://doi.org/10.1016/j.gloplacha.2018.04.007>.
- Crosta, X., Debret, M., Denis, D., Courty, M.A., Ther, O., 2007. Holocene long- and short-term climate changes off Adélie Land, East Antarctica. *Geochem. Geophys. Geosystems* 8. <https://doi.org/10.1029/2007GC001718> n/a-n/a.
- Crosta, X., Denis, D., Ther, O., 2008. Sea ice seasonality during the Holocene, Adélie Land, East Antarctica. *Marine Micropaleontology* 66, 222–232. <https://doi.org/10.1016/j.marmicro.2007.10.001>.
- Crosta, X., Romero, O., Armand, L., Pichon, J.-J., 2005. The biogeography of major diatom taxa in Southern Ocean sediments: 2. Open ocean related species. *Palaeogeogr. Palaeoclimatol. Palaeoecol.* 223 <https://doi.org/10.1016/j.palaeo.2005.03.028>.
- Cunningham, W.L., Leventer, A., 1998. Diatom assemblages in surface sediments of the Ross Sea: relationship to present oceanographic conditions. *Antarct. Sci.* 10, 134–146. <https://doi.org/10.1017/S0954102098000182>.
- Dätwyler, C., Neukom, R., Abram, N.J., Gallant, A.J.E., Grosjean, M., Jacques-Coper, M., Karoly, D.J., Villalba, R., 2018. Teleconnection stationarity, variability and trends of the Southern Annular Mode (SAM) during the last millennium. *Clim. Dyn.* 51, 2321–2339. <https://doi.org/10.1007/s00382-017-4015-0>.
- DeMaster, D.J., Ragueneau, O., Nittrouer, C.A., 1996. Preservation efficiencies and accumulation rates for biogenic silica and organic C, N, and P in high-latitude sediments: the Ross Sea. *J. Geophys. Res. Oceans* 101, 18501–18518. <https://doi.org/10.1029/96JC01634>.
- Denis, D., Crosta, X., Barbara, L., Massé, G., Renssen, H., Ther, O., Giraudeau, J., 2010. Sea ice and wind variability during the Holocene in East Antarctica: insight on middle–high latitude coupling. *Quat. Sci. Rev.* 29, 3709–3719. <https://doi.org/10.1016/j.quascirev.2010.08.007>.
- Denis, D., Crosta, X., Schmidt, S., Carson, D.S., Ganeshram, R.S., Renssen, H., Bout-Roumazelles, V., Zaragosi, S., Martin, B., Cremer, M., 2009a. Holocene glacier and deep water dynamics, Adélie Land region, East Antarctica. *Quaternary Science Reviews* 28, 1291–1303. <https://doi.org/10.1016/j.quascirev.2008.12.024>.
- Di Roberto, A., Colizza, E., Del Carlo, P., Petrelli, M., Finocchiaro, F., Kuhn, G., 2019. First marine cryptotephra in Antarctica found in sediments of the western Ross Sea correlates with englacial tephra and climate records. *Sci. Rep.* 9, 10628 <https://doi.org/10.1038/s41598-019-47188-3>.
- Domack, E., Leventer, A., Dunbar, R., Taylor, F., Brachfeld, S., Sjunneskog, C., Odp, 2001. Chronology of the Palmer Deep site, Antarctic Peninsula: a Holocene palaeoenvironmental reference for the circum-antarctic. *Holocene* 11, 1–9. <https://doi.org/10.1191/095968301673881493>.
- Domack, E.W., Jacobson, E.A., Shipp, S., Anderson, J.B., 1999. Late Pleistocene–Holocene retreat of the West Antarctic ice-sheet system in the Ross Sea: Part 2—sedimentologic and stratigraphic signature. *GSA Bull.* 111, 1517–1536. [https://doi.org/10.1130/0016-7606\(1999\)111<1517:LPHROT>2.3.CO;2](https://doi.org/10.1130/0016-7606(1999)111<1517:LPHROT>2.3.CO;2).
- Emslie, S.D., McKenzie, A., Patterson, W.P., 2018. The rise and fall of an ancient Adélie penguin ‘supercolony’ at Cape Adare, Antarctica. *R. Soc. Open Sci.* 5, 172032 <https://doi.org/10.1098/rsos.172032>.
- Domack, E.W., Ishman, S., 1993. Oceanographic and physiographic controls on modern sedimentation within Antarctic fjords. *GSA Bulletin* 105, 1175–1189. [https://doi.org/10.1130/0016-7606\(1993\)105<1175:OAPCOM>2.3.CO;2](https://doi.org/10.1130/0016-7606(1993)105<1175:OAPCOM>2.3.CO;2).
- Evans, D.J.A., Benn, D.I., 2014. *A Practical Guide to the Study of Glacial Sediments*. Routledge.
- Fernandez, A., Santos, G.M., Williams, E.K., Pendergraft, M.A., Vetter, L., Rosenheim, B.E., 2014. Blank corrections for ramped pyrolysis radiocarbon dating of sedimentary and soil organic carbon. *Anal. Chem.* 86, 12085–12092. <https://doi.org/10.1021/ac502874j>.
- Folk, R.L., Ward, W.C., 1957. Brazos River bar [Texas]; a study in the significance of grain size parameters. *J. Sediment. Res.* 27, 3–26. <https://doi.org/10.1306/74D70646-2B21-11D7-8648000102C1865D>.
- Gaglioti, B.V., Mann, D.H., Jones, B.M., Pohlman, J.W., Kunz, M.L., Wooller, M.J., 2014. Radiocarbon age-offsets in an arctic lake reveal the long-term response of permafrost carbon to climate change. *J. Geophys. Res. Biogeosciences* 119, 1630–1651. <https://doi.org/10.1002/2014JG002688>.
- Gao, M., Kim, S.-J., Yang, J., Liu, J., Jiang, T., Su, B., Wang, Y., Huang, J., 2021. Historical fidelity and future change of Amundsen Sea Low under 1.5°C–4°C global warming in CMIP6. *Atmos. Res.*, 105533 <https://doi.org/10.1016/j.atmosres.2021.105533>.
- Gao, Y., Salvatore, M.C., Xu, Q., Yang, L., Sun, L., Xie, Z., Baroni, C., 2022. The occupation history of the longest-dwelling Adélie penguin colony reflects Holocene climatic and environmental changes in the Ross Sea, Antarctica. *Quat. Sci. Rev.* 284, 107494 <https://doi.org/10.1016/j.quascirev.2022.107494>.
- Geilfus, N.-X., Galley, R.J., Crabeck, O., Papakyriakou, T., Landy, J., Tison, J.-L., Rysgaard, S., 2015. Inorganic carbon dynamics of melt-pond-covered first-year sea ice in the Canadian Arctic. *Biogeosciences* 12, 2047–2061. <https://doi.org/10.5194/bg-12-2047-2015>.
- Gersonde, R., Zielinski, U., 2000. The reconstruction of late Quaternary Antarctic sea-ice distribution—the use of diatoms as a proxy for sea-ice. *Palaeogeogr. Palaeoclimatol. Palaeoecol.* 162, 263–286. [https://doi.org/10.1016/S0031-0182\(00\)00131-0](https://doi.org/10.1016/S0031-0182(00)00131-0).

- Gibson, J.A.E., Trull, T., Nichols, P.D., Summons, R.E., McMin, A., 1999. Sedimentation of ^{13}C -rich organic matter from Antarctic sea-ice algae: a potential indicator of past sea-ice extent. *Geology* 27, 331. [https://doi.org/10.1130/0091-7613\(1999\)027<0331:SOCROM>2.3.CO;2](https://doi.org/10.1130/0091-7613(1999)027<0331:SOCROM>2.3.CO;2).
- Ginnane, C.E., Turnbull, J.C., Naeher, S., Rosenheim, B.E., Venturelli, R.A., Phillips, A. M., Reeve, S., Parry-Thompson, J., Zondervan, A., Levy, R.H., Yoo, K.-C., Dunbar, G., Calkin, T., Escutia, C., Pastor, J.G., 2024. Advancing Antarctic sediment chronology through combined ramped pyrolysis oxidation and pyrolysis-GC-MS. *Radiocarbon* 1–20. <https://doi.org/10.1017/RDC.2023.116>.
- Goodwin, I., Browning, S., Lorrey, A., A. Mayewski, P., J. Phipps, S., Bertler, N., Edwards, R., Cohen, T., Van Ommen, T., Curran, M., Barr, C., Stager, J., 2014. A reconstruction of extratropical Indo-Pacific sea-level pressure patterns during the Medieval Climate Anomaly. *Clim. Dyn.* 43, 1197–1219. <https://doi.org/10.1007/s00382-013-1899-1>.
- Gordon, A.L., Huber, B.A., Buseck, J., 2015. Bottom water export from the western Ross Sea, 2007 through 2010. *Geophys. Res. Lett.* 42, 5387–5394. <https://doi.org/10.1002/2015GL064457>.
- Halberstadt, A.R.W., Simkins, L.M., Greenwood, S.L., Anderson, J.B., 2016. Past ice-sheet behaviour: retreat scenarios and changing controls in the Ross Sea, Antarctica. *Cryosphere* 10, 1003–1020. <https://doi.org/10.5194/tc-10-1003-2016>.
- Hall, B.L., Henderson, G.M., Baroni, C., Kellogg, T.B., 2010. Constant Holocene Southern-Ocean ^{14}C reservoir ages and ice-shelf flow rates. *Earth Planet Sci. Lett.* 296, 115–123. <https://doi.org/10.1016/j.epsl.2010.04.054>.
- Haslett, J., Parnell, A., 2008. A simple monotone process with application to radiocarbon-dated depth chronologies. *J. R. Stat. Soc. Ser. C Appl. Stat.* 57, 399–418.
- Heaton, T.J., Butzin, M., Bard, E., et al., 2023. Marine Radiocarbon Calibration in Polar Regions: A Simple Approximate Approach using Marine2. *Radiocarbon* 65 (4), 848–875. <https://doi.org/10.1017/RDC.2023.42>.
- Heaton, T.J., Köhler, P., Butzin, M., Bard, E., Reimer, R.W., Austin, W.E.N., Ramsey, C.B., Grootes, P.M., Hughen, K.A., Kromer, B., Reimer, P.J., Adkins, J., Burke, A., Cook, M. S., Olsen, J., Skinner, L.C., 2020. Marine20—the marine radiocarbon age calibration curve (0–55,000 cal BP). *Radiocarbon* 62, 779–820. <https://doi.org/10.1017/RDC.2020.68>.
- Hemer, M.A., Harris, P.T., 2003. Sediment core from beneath the Amery Ice Shelf, East Antarctica, suggests mid-Holocene ice-shelf retreat. *Geology* 31, 127–130. [https://doi.org/10.1130/0091-7613\(2003\)031<0127:SCFBTA>2.0.CO;2](https://doi.org/10.1130/0091-7613(2003)031<0127:SCFBTA>2.0.CO;2).
- Henke, L.M.K., Lambert, F.H., Charman, D.J., 2017. Was the Little Ice Age more or less El Niño-like than the Medieval Climate Anomaly? Evidence from hydrological and temperature proxy data. *Clim. Past* 13, 267–301. <https://doi.org/10.5194/cp-13-267-2017>.
- Henley, S.F., Annett, A.L., Ganeshram, R.S., Carson, D.S., Weston, K., Crosta, X., Tait, A., Dougans, J., Fallick, A.E., Clarke, A., 2012. Factors influencing the stable carbon isotopic composition of suspended and sinking organic matter in the coastal Antarctic sea ice environment. *Biogeosciences* 9, 1137–1157. <https://doi.org/10.5194/bg-9-1137-2012>.
- Hillenbrand, C.-D., Bentley, M.J., Stollard, T.D., Hein, A.S., Kuhn, G., Graham, A.G.C., Fogwill, C.J., Kristoffersen, Y., Smith, James A., Anderson, J.B., Larter, R.D., Melles, M., Hodgson, D.A., Mulvaney, R., Sugden, D.E., 2014. Reconstruction of changes in the Weddell Sea sector of the Antarctic Ice Sheet since the Last Glacial Maximum. *Quat. Sci. Rev.*, Reconstruction of Antarctic Ice Sheet Deglaciation (RAISED) 100, 111–136. <https://doi.org/10.1016/j.quascirev.2013.07.020>.
- Hillenbrand, C.-D., Smith, J.A., Kuhn, G., Esper, O., Gersonde, R., Larter, R.D., Maher, B., Moreton, S.G., Shimmield, T.M., Korte, M., 2010. Age assignment of a diatomaceous ooze deposited in the western Amundsen Sea Embayment after the Last Glacial Maximum. *J. Quat. Sci.* 25, 280–295. <https://doi.org/10.1002/jqs.1308>.
- Hinojosa, J.L., Moy, C.M., Stirling, C.H., Wilson, G.S., Eglinton, T.I., 2017. A New Zealand perspective on centennial-scale Southern Hemisphere westerly wind shifts during the last two millennia. *Quat. Sci. Rev.* 172, 32–43. <https://doi.org/10.1016/j.quascirev.2017.07.016>.
- Höfer, J., Giesecke, R., Hopwood, M.J., Carrera, V., Alarcón, E., González, H.E., 2019. The role of water column stability and wind mixing in the production/export dynamics of two bays in the Western Antarctic Peninsula. *Prog. Oceanogr.*, Subantarctic and Antarctic Marine Ecosystems: outlining patterns and processes in a changing ocean 174, 105–116. <https://doi.org/10.1016/j.pocean.2019.01.005>.
- Jacobs, S.S., Giulivi, C.F., Dutrieux, P., 2022. Persistent Ross Sea freshening from imbalance West Antarctic ice shelf melting. *J. Geophys. Res. Oceans* 127, e2021JC017808. <https://doi.org/10.1029/2021JC017808>.
- Jin, J., Chen, X., Xu, L., Nie, Y., Wang, X., Huang, H., Emslie, S.D., Liu, X., 2021. Chronology and paleoclimatic implications of lacustrine sediments at Inexpressible Island, Ross Sea, Antarctica. *Palaeogeogr. Palaeoclimatol. Palaeoecol.* 576, 110497. <https://doi.org/10.1016/j.palaeo.2021.110497>.
- Johnson, K.M., McKay, R.M., Etourneau, J., Jiménez-Espejo, F.J., Albot, A., Riesselman, C.R., Bertler, N.A.N., Horgan, H.J., Crosta, X., Bendle, J., Ashley, K.E., Yamane, M., Yokoyama, Y., Pekar, S.F., Escutia, C., Dunbar, R.B., 2021. Sensitivity of Holocene East Antarctic productivity to subdecadal variability set by sea ice. *Nat. Geosci.* <https://doi.org/10.1038/s41561-021-00816-y>.
- Jones, J.M., Gille, S.T., Goosse, H., Abram, N.J., Canziani, P.O., Charman, D.J., Clem, K. R., Crosta, X., de Lavergne, C., Eisenman, I., England, M.H., Fogt, R.L., Frankcombe, L.M., Marshall, G.J., Masson-Delmotte, V., Morrison, A.K., Orsi, A.J., Raphael, M.N., Renwick, J.A., Schneider, D.P., Simkins, G.R., Steig, E.J., Stenni, B., Swingedouw, D., Vance, T.R., 2016. Assessing recent trends in high-latitude Southern Hemisphere surface climate. *Nat. Clim. Change* 6, 917–926. <https://doi.org/10.1038/nclimate3103>.
- Jones, R.S., Whitmore, R.J., Mackintosh, A.N., Norton, K.P., Eaves, S.R., Stutz, J., Christl, M., 2020. Regional-scale abrupt Mid-Holocene ice sheet thinning in the western Ross Sea, Antarctica. *Geology* 49, 278–282. <https://doi.org/10.1130/G48347.1>.
- Kim, J.-H., Crosta, X., Willmott, V., Renssen, H., Bonnin, J., Helmke, P., Schouten, S., Sinninghe Damsté, J.S., 2012. Holocene subsurface temperature variability in the eastern Antarctic continental margin. *Geophys. Res. Lett.* 39. <https://doi.org/10.1029/2012GL051157>.
- Kim, S., Yoo, K.-C., Lee, J.I., Khim, B.-K., Bak, Y.-S., Lee, M.K., Lee, J., Domack, E.W., Christ, A.J., Yoon, H.I., 2018. Holocene paleoceanography of Bigo Bay, West Antarctic Peninsula: connections between surface water productivity and nutrient utilization and its implication for surface-deep water mass exchange. *Quat. Sci. Rev.* 192, 59–70. <https://doi.org/10.1016/j.quascirev.2018.05.028>.
- King, J., Anchukaitis, K.J., Allen, K., Vance, T., Hessel, A., 2023. Trends and variability in the Southern Annular Mode over the Common Era. *Nat. Commun.* 14, 2324. <https://doi.org/10.1038/s41467-023-37643-1>.
- King, T.M., Rosenheim, B.E., Post, A.L., Gabris, T., Burt, T., Domack, E.W., 2018. Large-scale intrusion of Circumpolar Deep Water on Antarctic margin recorded by stylasterid corals. *Paleoceanogr. Paleoclimatol.* 33, 1306–1321. <https://doi.org/10.1029/2018PA003439>.
- Koffman, B.G., Goldstein, S.L., Winckler, G., Kaplan, M.R., Bolje, L., Biscaye, P., 2023. Abrupt changes in atmospheric circulation during the Medieval Climate Anomaly and Little Ice Age recorded by Sr-Nd isotopes in the Siple Dome ice core, Antarctica. *Paleoceanogr. Paleoclimatol.* 38, e2022PA004543. <https://doi.org/10.1029/2022PA004543>.
- Koffman, B.G., Kreuz, K.J., Breton, D.J., Kane, E.J., Winski, D.A., Birkel, S.D., Kurbatov, A.V., Handley, M.J., 2014. Centennial-scale variability of the Southern Hemisphere westerly wind belt in the eastern Pacific over the past two millennia. *Clim. Past* 10, 1125–1144. <https://doi.org/10.5194/cp-10-1125-2014>.
- Kyle, P.R., 1990. A McMurdo volcanic Group western Ross Embayment. In: *Volcanoes of the Antarctic Plate and Southern Oceans*. American Geophysical Union (AGU), pp. 18–145. <https://doi.org/10.1029/AR048p0018>.
- Leventer, A., 1992. Modern distribution of diatoms in sediments from the George V Coast, Antarctica. *Mar. Micropaleontol.* 19, 315–332. [https://doi.org/10.1016/0377-8398\(92\)90036-J](https://doi.org/10.1016/0377-8398(92)90036-J).
- Laskar, J., Robutel, P., Joutel, F., Gastineau, M., Correia, A.C.M., Levrard, B., 2004. A long-term numerical solution for the insolation quantities of the Earth. *A&A* 428, 261–285. <https://doi.org/10.1051/0004-6361:20041335>.
- Leventer, A., Domack, E.W., Ishman, S.E., Brachfeld, S., McClennen, C.E., Manley, P., 1996. Productivity cycles of 200–300 years in the Antarctic Peninsula region: understanding linkages among the sun, atmosphere, oceans, sea ice, and biota. *GSA Bull.* 108, 1626–1644. [https://doi.org/10.1130/0016-7606\(1996\)108<1626:PCOYIT>2.3.CO;2](https://doi.org/10.1130/0016-7606(1996)108<1626:PCOYIT>2.3.CO;2).
- Leventer, A., Dunbar, R.B., 1996. Factors influencing the distribution of diatoms and other algae in the Ross Sea. *J. Geophys. Res. Oceans* 101, 18489–18500. <https://doi.org/10.1029/96JC00204>.
- Li, Q., England, M.H., Hogg, A.M., Rintoul, S.R., Morrison, A.K., 2023. Abyssal ocean overturning slowdown and warming driven by Antarctic meltwater. *Nature* 615, 841–847. <https://doi.org/10.1038/s41586-023-05762-w>.
- Lüning, S., Gaika, M., Vahrenholt, F., 2019. The Medieval Climate Anomaly in Antarctica. *Palaeogeogr. Palaeoclimatol. Palaeoecol.* 532, 109251. <https://doi.org/10.1016/j.palaeo.2019.109251>.
- Marshall, G., 2003. Trends in the Southern Annular Mode from observations and reanalyses. *J. Clim.* 16, 4134–4143. [https://doi.org/10.1175/1520-0442\(2003\)016<4134:TTSAM>2.0.CO;2](https://doi.org/10.1175/1520-0442(2003)016<4134:TTSAM>2.0.CO;2).
- McKay, R., Albot, O., Dunbar, G.B., Lee, J.I., Lee, M.K., Yoo, K., Kim, S., Turton, N., Kulhanek, D., Patterson, M., Levy, R., 2022. A comparison of methods for identifying and quantifying ice rafted debris on the Antarctic margin. *Paleoceanogr. Paleoclimatol.* 37. <https://doi.org/10.1029/2021PA004404>.
- McKay, R., Golledge, N.R., Maas, S., Naish, T., Levy, R., Dunbar, G., Kuhn, G., 2016. Antarctic marine ice-sheet retreat in the Ross Sea during the early Holocene. *Geology* 44, 7–10. <https://doi.org/10.1130/G37315.1>.
- McKay, R.M., De Santis, L., Kulhanek, D.K., 2019. Ross Sea West Antarctic ice sheet history. Proceedings of the International Ocean Discovery Program. International Ocean Discovery Program. <https://doi.org/10.14379/iodp.proc.374.2019>.
- McKay, R.M., Dunbar, G.B., Naish, T.R., Barrett, P.J., Carter, L., Harper, M., 2008. Retreat history of the Ross Ice Sheet (Shelf) since the Last Glacial Maximum from deep-basin sediment cores around Ross Island. *Paleoceanogr. Paleoclimatol. Palaeoecol.* 260, 245–261. <https://doi.org/10.1016/j.palaeo.2007.08.015>.
- Mezgec, K., Stenni, B., Crosta, X., Masson-Delmotte, V., Baroni, C., Braidia, M., Ciardini, V., Colizza, E., Melis, R., Salvatore, M.C., Severi, M., Scarchilli, C., Traversi, R., Udisti, R., Frezzotti, M., 2017. Holocene sea ice variability driven by wind and polynya efficiency in the Ross Sea. *Nat. Commun.* 8, 1334. <https://doi.org/10.1038/s41467-017-01455-x>.
- Miles, B.W.J., Stokes, C.R., Jamieson, S.S.R., 2016. Pan-ice-sheet glacier terminus change in East Antarctica reveals sensitivity of Wilkes Land to sea-ice changes. *Sci. Adv.* 2, e1501350. <https://doi.org/10.1126/sciadv.1501350>.
- Minzoni, R.T., Anderson, J.B., Fernandez, R., Wellner, J.S., 2015. Marine record of Holocene climate, ocean, and cryosphere interactions: Herbert Sound, James Ross Island, Antarctica. *Quat. Sci. Rev.* 129, 239–259. <https://doi.org/10.1016/j.quascirev.2015.09.009>.
- Morrison, A.K., Hogg, A.M., England, M.H., Spence, P., 2020. Warm Circumpolar Deep Water transport toward Antarctica driven by local dense water export in canyons. *Sci. Adv.* 6, eaav2516. <https://doi.org/10.1126/sciadv.aav2516>.
- Mortlock, R.A., Froelich, P.N., 1989. A simple method for the rapid determination of biogenic opal in pelagic marine sediments. *Deep-Sea Res. Part A Oceanogr. Res. Pap.* 36, 1415–1426. [https://doi.org/10.1016/0198-0149\(89\)90092-7](https://doi.org/10.1016/0198-0149(89)90092-7).

- Mulvaney, R., Abram, N.J., Hindmarsh, R.C.A., Arrowsmith, C., Fleet, L., Triest, J., Sime, L.C., Alemany, O., Foord, S., 2012. Recent Antarctic Peninsula warming relative to Holocene climate and ice-shelf history. *Nature* 489, 141–144. <https://doi.org/10.1038/nature11391>.
- Naeher, S., Gilli, A., North, R.P., Hamann, Y., Schubert, C.J., 2013. Tracing bottom water oxygenation with sedimentary Mn/Fe ratios in Lake Zurich, Switzerland. *Chem. Geol.* 9.
- Neuhaus, S.U., Tulaczyk, S.M., Stansell, N.D., Coenen, J.J., Scherer, R.P., Mikucki, J.A., Powell, R.D., 2021. Did Holocene climate changes drive West Antarctic grounding line retreat and readvance? *Cryosphere* 15, 4655–4673. <https://doi.org/10.5194/15-4655-2021>.
- Neukom, R., Barboza, L.A., Erb, M.P., Shi, F., Emile-Geay, J., Evans, M.N., Franke, J., Kaufman, D.S., Lücke, L., Rehfeld, K., Schurer, A., Zhu, F., Brönnimann, S., Hakim, G.J., Henley, B.J., Ljungqvist, F.C., McKay, N., Valler, V., von Gunten, L., Pages, 2k Consortium, 2019. Consistent multidecadal variability in global temperature reconstructions and simulations over the Common Era. *Nat. Geosci.* 12, 643–649. <https://doi.org/10.1038/s41561-019-0400-0>.
- Ó Cofaigh, C., Davies, B.J., Livingstone, S.J., Smith, J.A., Johnson, J.S., Hocking, E.P., Hodgson, D.A., Anderson, J.B., Bentley, M.J., Canals, M., Domack, E., Dowdeswell, J. A., Evans, J., Glasser, N.F., Hillenbrand, C.-D., Larter, R.D., Roberts, S.J., Simms, A. R., 2014. Reconstruction of ice-sheet changes in the Antarctic Peninsula since the Last Glacial Maximum. *Quat. Sci. Rev.*, Reconstruction of Antarctic Ice Sheet Deglaciation (RAISED) 100, 87–110. <https://doi.org/10.1016/j.quascirev.2014.06.023>.
- Orsi, A.J., Cornuelle, B.D., Severinghaus, J.P., 2012. Little Ice Age cold interval in West Antarctica: evidence from borehole temperature at the West Antarctic Ice Sheet (WAIS) divide. *Geophys. Res. Lett.* 39 <https://doi.org/10.1029/2012GL051260>.
- Orsi, A.H., Wiederwohl, C.L., 2009. A recount of Ross Sea waters. *Deep Sea Research Part II. Topical Studies in Oceanography, Southern Ocean Shelf Slope Exchange* 56, 778–795. <https://doi.org/10.1016/j.dsr2.2008.10.033>.
- Otto-Bliessner, B.L., Brady, E.C., Fasullo, J., Jahn, A., Landrum, L., Stevenson, S., Rosenbloom, N., Mai, A., Strand, G., 2015. Climate variability and change since 850 CE: an ensemble approach with the Community Earth System Model. *Bull. Am. Meteorol. Soc.* 97, 735–754. <https://doi.org/10.1175/BAMS-D-14-00233.1>.
- Panizzo, V., Crespin, J., Crosta, X., Shemesh, A., Massé, G., Yam, R., Mattioli, N., Cardinal, D., 2014. Sea ice diatom contributions to Holocene nutrient utilization in East Antarctica. *Paleoceanography* 29, 328–343. <https://doi.org/10.1002/2014PA002609>.
- Parker, R.L., 2017. *Sea ice extent and diatom primary production within the SW Ross Sea, Antarctica: the response to post-glacial warming*. [Master's thesis, University of Otago].
- Peck, V.L., Allen, C.S., Kender, S., McClymont, E.L., Hodgson, D.A., 2015. Oceanographic variability on the West Antarctic Peninsula during the Holocene and the influence of upper circumpolar deep water. *Quat. Sci. Rev.* 119, 54–65. <https://doi.org/10.1016/j.quascirev.2015.04.002>.
- Pedregosa, F., Varoquaux, G., Gramfort, A., Michel, V., Thirion, B., Grisel, O., Blondel, M., Prettenhofer, P., Weiss, R., Dubourg, V., Vanderplas, J., 2011. Scikit-learn: Machine learning in Python. *The Journal of machine Learning research* 12, 2825–2830.
- Pendergraft, M.A., Dincer, Z., Sericano, J.L., Wade, T.L., Kolasinski, J., Rosenheim, B.E., 2013. Linking ramped pyrolysis isotope data to oil content through PAH analysis. *Environ. Res. Lett.* 8, 044038 <https://doi.org/10.1088/1748-9326/8/4/044038>.
- Pendergraft, M.A., Rosenheim, B.E., 2014. Varying relative degradation rates of oil in different forms and environments revealed by ramped pyrolysis. *Environ. Sci. Technol.* 48, 10966–10974. <https://doi.org/10.1021/es501354c>.
- Perren, B.B., Hodgson, D.A., Roberts, S.J., Sime, L., Van Nieuwenhuyze, W., Verleyen, E., Vyverman, W., 2020. Southward migration of the Southern Hemisphere westerly winds corresponds with warming climate over centennial timescales. *Commun. Earth Environ.* 1, 1–8. <https://doi.org/10.1038/s43247-020-00059-6>.
- Pike, J., Crosta, X., Maddison, E.J., Stickley, C.E., Denis, D., Barbara, L., Renssen, H., 2009. Observations on the relationship between the Antarctic coastal diatoms *Thalassiosira antarctica* Comber and *Porosira glacialis* (Grunow) Jørgensen and sea ice concentrations during the late Quaternary. *Mar. Micropaleontol.* 73, 14–25. <https://doi.org/10.1016/j.marmicro.2009.06.005>.
- Pritchard, H.D., Ligtenberg, S.R.M., Fricker, H.A., Vaughan, D.G., van den Broeke, M.R., Padman, L., 2012. Antarctic ice-sheet loss driven by basal melting of ice shelves. *Nature* 484, 502–505. <https://doi.org/10.1038/nature10968>.
- Reback, J., W.Jbrockmendel, McKinney, Bossche, J.V.D., Augspurger, T., Cloud, P., Gfyoung, Sinhrks, Klein, A., Roeschke, M., Hawkins, S., Tratner, J., She, C., Ayd, W., Terji, Petersen, Garcia, M., Schendel, J., A.MomIsBestFriend, Hayden, Jancauskas, V., Battiston, P., SeaboldChris-B, Skipper, Vetinari, H., Hoyer, S., Overmeire, W., Alimcmaster, Kaiqi Dong, Whelan, C., Mortada, Mehvar, 2020. pandas-dev/pandas: pandas 1.0.3. <https://doi.org/10.5281/ZENODO.3715232>.
- Rhee, H.H., Lee, M.K., Seong, Y.B., Lee, J.I., Yoo, K.-C., Yu, B.Y., 2020. Post-LGM dynamic deglaciation along the Victoria Land coast, Antarctica. *Quat. Sci. Rev.* 247, 106595 <https://doi.org/10.1016/j.quascirev.2020.106595>.
- Rhodes, R.H., Bertler, N.A.N., Baker, J.A., Steen-Larsen, H.C., Sneed, S.B., Morgenstern, U., Johnsen, S.J., 2012. Little Ice Age climate and oceanic conditions of the Ross Sea, Antarctica from a coastal ice core record. *Clim. Past* 8, 1223–1238. <https://doi.org/10.5194/cp-8-1223-2012>.
- Rignot, E., Mouginot, J., Scheuchl, B., van den Broeke, M., van Wessem, M.J., Morlighem, M., 2019. Four decades of Antarctic Ice Sheet mass balance from 1979–2017. *Proc. Natl. Acad. Sci.* 116, 1095–1103. <https://doi.org/10.1073/pnas.1812883116>.
- Rosenheim, B.E., Day, M.B., Domack, E., Schrum, H., Benthien, A., Hayes, J.M., 2008. Antarctic sediment chronology by programmed-temperature pyrolysis: methodology and data treatment. *Geochem. Geophys. Geosystems* 9. <https://doi.org/10.1029/2007GC001816>.
- Rosenheim, B.E., Galy, V., 2012. Direct measurement of riverine particulate organic carbon age structure. *Geophys. Res. Lett.* 39 <https://doi.org/10.1029/2012GL052883>.
- Rosenheim, B.E., Roe, K.M., Roberts, B.J., Kolker, A.S., Allison, M.A., Johannsson, K.H., 2013a. River discharge influences on particulate organic carbon age structure in the Mississippi/Atchafalaya River System. *Glob. Biogeochem. Cycles* 27, 154–166. <https://doi.org/10.1002/gbc.20018>.
- Rosenheim, B.E., Santoro, J.A., Gunter, M., Domack, E.W., 2013b. Improving Antarctic Sediment ¹⁴C Dating Using Ramped Pyrolysis: An Example from the Hugo Island Trough. *Radiocarbon* 55, 115–126.
- Sadai, S., Condron, A., DeConto, R., Pollard, D., 2020. Future climate response to Antarctic Ice Sheet melt caused by anthropogenic warming. *Science Advances* 6, eaaz1169. <https://doi.org/10.1126/sciadv.aaz1169>.
- Schine, C.M.S., Dijken, G. van, Arrigo, K.R., 2016. Spatial analysis of trends in primary production and relationship with large-scale climate variability in the Ross Sea, Antarctica (1997–2013). *J. Geophys. Res. Oceans* 121, 368–386. <https://doi.org/10.1002/2015JC011014>.
- Schreiner, K.M., Bianchi, T.S., Rosenheim, B.E., 2014. Evidence for permafrost thaw and transport from an Alaskan North Slope watershed. *Geophys. Res. Lett.* 41, 3117–3126. <https://doi.org/10.1002/2014GL059514>.
- Shevenell, A.E., Ingalls, A.E., Domack, E.W., Kelly, C., 2011. Holocene Southern Ocean surface temperature variability west of the Antarctic Peninsula. *Nature* 470, 250–254. <https://doi.org/10.1038/nature09751>.
- Siebert, M.J., Kingslake, J., Ross, N., Whitehouse, P.L., Woodward, J., Jamieson, S.S.R., Bentley, M.J., Winter, K., Wearing, M., Hein, A.S., Jeofry, H., Sugden, D.E., 2019. Major ice sheet change in the Weddell sea sector of West Antarctica over the last 5,000 years. *Rev. Geophys.* 57, 1197–1223. <https://doi.org/10.1029/2019RG000651>.
- Silvano, A., Rintoul, S.R., Peña-Molino, B., Williams, G.D., 2017. Distribution of water masses and meltwater on the continental shelf near the Totten and Moscow University ice shelves. *J. Geophys. Res.: Oceans* 122, 2050–2068. <https://doi.org/10.1002/2016JC012115>.
- Silvano, A., Rintoul, S.R., Peña-Molino, B., Hobbs, W.R., Wijk, E. van, Aoki, S., Tamura, T., Williams, G.D., 2018. Freshening by glacial meltwater enhances melting of ice shelves and reduces formation of Antarctic Bottom Water. *Sci. Adv.* 4, eaap9467 <https://doi.org/10.1126/sciadv.aap9467>.
- Simms, A.R., Bentley, M.J., Simkins, L.M., Zurbuchen, J., Reynolds, L.C., DeWitt, R., Thomas, E.R., 2021. Evidence for a “Little Ice Age” glacial advance within the Antarctic Peninsula – examples from glacially-overnun raised beaches. *Quat. Sci. Rev.* 271, 107195 <https://doi.org/10.1016/j.quascirev.2021.107195>.
- Smith, J.A., Graham, A.G.C., Post, A.L., Hillenbrand, C.-D., Bart, P.J., Powell, R.D., 2019. The marine geological imprint of Antarctic ice shelves. *Nat. Commun.* 10, 1–16. <https://doi.org/10.1038/s41467-019-13496-5>.
- Spector, P., Stone, J., Cowdery, S.G., Hall, B., Conway, H., Bromley, G., 2017. Rapid early-Holocene deglaciation in the Ross Sea, Antarctica: early-Holocene Ross Sea deglaciation. *Geophys. Res. Lett.* 44, 7817–7825. <https://doi.org/10.1002/2017GL074216>.
- Spence, P., Griffies, S.M., England, M.H., Hogg, A.McC., Saenko, O.A., Jourdain, N.C., 2014. Rapid subsurface warming and circulation changes of Antarctic coastal waters by poleward shifting winds: Antarctic subsurface ocean warming. *Geophys. Res. Lett.* 41, 4601–4610. <https://doi.org/10.1002/2014GL060613>.
- Stammerjohn, S.E., Martinson, D.G., Smith, R.C., Yuan, X., Rind, D., 2008. Trends in Antarctic annual sea ice retreat and advance and their relation to El Niño–Southern oscillation and Southern Annular Mode variability. *J. Geophys. Res. Oceans* 113. <https://doi.org/10.1029/2007JC004269>.
- Stenni, B., Curran, M.A.J., Abram, N.J., Orsi, A., Goursaud, S., Masson-Delmotte, V., Neukom, R., Goosse, H., Divine, D., van Ommen, T., Steig, E.J., Dixon, D.A., Thomas, E.R., Bertler, N.A.N., Isaksson, E., Ekaykin, A., Werner, M., Frezzotti, M., 2017. Antarctic climate variability on regional and continental scales over the last 20,000 years. *Clim. Past* 13, 1609–1634. <https://doi.org/10.5194/cp-13-1609-2017>.
- Stoll, H.M., Mendez-Vicente, A., Abrevaya, L., Anderson, R.F., Rigual-Hernández, A.S., Gonzalez-Lemos, S., 2017. Growth rate and size effect on carbon isotopic fractionation in diatom-bound organic matter in recent Southern Ocean sediments. *Earth Planet Sci. Lett.* 457, 87–99. <https://doi.org/10.1016/j.epsl.2016.09.028>.
- Strickland, J.D.H., Parsons, T.R., 1972. *A Practical Handbook of Seawater Analysis*, 2nd edition. <https://doi.org/10.25607/OBP-1791>.
- Subt, C., Fangman, K.A., Wellner, J.S., Rosenheim, B.E., 2016. Sediment chronology in Antarctic deglacial sediments: reconciling organic carbon ¹⁴C ages to carbonate ¹⁴C ages using Ramped PyrOx. *Holocene* 26, 265–273. <https://doi.org/10.1177/0959683615608688>.
- Subt, C., I. Yoon, H., Yoo, K.-C., Lee, J.I., Leventer, A., Domack, E., Rosenheim, B., 2017. Sub-ice shelf sediment geochronology utilizing novel radiocarbon methodology for detrital-rich sediments. *Geochem. Geophys. Geosystems*. <https://doi.org/10.1002/2016GC006578>.
- Taylor, F., Whitehead, J., Domack, E., 2001. Holocene paleoclimate change in the Antarctic Peninsula: evidence from the diatom, sedimentary and geochemical record. *Mar. Micropaleontol.* 41, 25–43. [https://doi.org/10.1016/S0377-8398\(00\)00049-9](https://doi.org/10.1016/S0377-8398(00)00049-9).
- Tesi, T., Belt, S.T., Gariboldi, K., Muschitiello, F., Smik, L., Finocchiaro, F., Giglio, F., Colizza, E., Gazzurra, G., Giordano, P., Morigi, C., Capotondi, L., Nogarotto, A., Köseoglu, D., Di Roberto, A., Gallerani, A., Langone, L., 2020. Resolving sea ice dynamics in the north-western Ross Sea during the last 2.6 ka: from seasonal to millennial timescales. *Quat. Sci. Rev.* 237, 106299 <https://doi.org/10.1016/j.quascirev.2020.106299>.

- Thompson, A.F., Stewart, A.L., Spence, P., Heywood, K.J., 2018. The Antarctic Slope current in a changing climate. *Rev. Geophys.* 56, 741–770. <https://doi.org/10.1029/2018RG000624>.
- Totten, R.L., Fonseca, A.N.R., Wellner, J.S., Munoz, Y.P., Anderson, J.B., Tobin, T.S., Lehrmann, A.A., 2022. Oceanographic and climatic influences on Trooz Glacier, Antarctica during the Holocene. *Quat. Sci. Rev.* 276, 107279 <https://doi.org/10.1016/j.quascirev.2021.107279>.
- Truax, O.J., Otto-Bliesner, B.L., Brady, E.C., Stevens, C.L., Wilson, G.S., Riesselman, C.R., 2022. Drivers of last millennium Antarctic climate evolution in an ensemble of Community Earth System Model simulations. *Geosciences* 12, 299. <https://doi.org/10.3390/geosciences12080299>.
- Turnbull, J.C., Zondervan, A., Kaiser, J., Norris, M., Dahl, J., Baisden, T., Lehman, S., 2015. High-precision atmospheric ^{14}C measurement at the Rafters Radiocarbon Laboratory. *Radiocarbon* 57, 377–388. https://doi.org/10.2458/azu_rc.57.18390.
- Venturelli, R.A., Siegfried, M.R., Roush, K.A., Li, W., Burnett, J., Zook, R., Fricker, H.A., Prisco, J.C., Leventer, A., Rosenheim, B.E., 2020. Mid-Holocene grounding line retreat and readvance at Whillans ice stream, west Antarctica. *Geophys. Res. Lett.* 47, e2020GL088476 <https://doi.org/10.1029/2020GL088476>.
- Vetter, L., Rosenheim, B.E., Fernandez, A., Törnqvist, T.E., 2017. Short organic carbon turnover time and narrow ^{14}C age spectra in early Holocene wetland paleosols. *Geochem. Geophys. Geosystems* 18, 142–155. <https://doi.org/10.1002/2016GC006526>.
- Villinski, J., B. Dunbar, R., Mucciaroni, D., 2000. Carbon 13/Carbon 12 ratios of sedimentary organic matter from the Ross Sea, Antarctica: a record of phytoplankton bloom dynamics. *J. Geophys. Res.* 105, 14163–14172. <https://doi.org/10.1029/1999JC000309>.
- Warner, N.R., Domack, E.W., 2002. Millennial- to decadal-scale paleoenvironmental change during the Holocene in the Palmer Deep, Antarctica, as recorded by particle size analysis. *Paleoceanography* 17. <https://doi.org/10.1029/2000PA000602>, 5-1-PAL 5-14.
- Warnock, J., Scherer, R., 2015. A revised method for determining the absolute abundance of diatoms. *J. Paleolimnol.* 53, 157–163. <https://doi.org/10.1007/s10933-014-9808-0>.
- Williams, E.K., Rosenheim, B.E., Allison, M., McNichol, A.P., Xu, L., 2015. Quantification of refractory organic material in Amazon mudbanks of the French Guiana Coast. *Mar. Geol.* 363, 93–101. <https://doi.org/10.1016/j.margeo.2015.02.009>.
- Williams, G.D., Aoki, S., Jacobs, S.S., Rintoul, S.R., Tamura, T., Bindoff, N.L., 2010. Antarctic bottom water from the Adélie and George V Land coast, East Antarctica (140–149°E). *J. Geophys. Res. Oceans* 115. <https://doi.org/10.1029/2009JC005812>.
- Winton, V.H.L., Dunbar, G.B., Bertler, N.A.N., Millet, M.-A., Delmonte, B., Atkins, C.B., Chewings, J.M., Andersson, P., 2014. The contribution of aeolian sand and dust to iron fertilization of phytoplankton blooms in southwestern Ross Sea, Antarctica. *Glob. Biogeochem. Cycles* 28, 423–436. <https://doi.org/10.1002/2013GB004574>.
- Wise, M.G., Dowdeswell, J.A., Jakobsson, M., Larter, R.D., 2017. Evidence of marine ice-cliff instability in Pine Island Bay from iceberg-keel plough marks. *Nature* 550, 506–510. <https://doi.org/10.1038/nature24458>.
- Xu, Q.B., Yang, L.J., Gao, Y.S., Sun, L.G., Xie, Z.Q., 2021. 6,000-Year reconstruction of Modified Circumpolar Deep Water intrusion and its effects on sea ice and penguin in the Ross Sea. *Geophys. Res. Lett.* 48, e2021GL094545 <https://doi.org/10.1029/2021GL094545>.
- Yuan, X., 2004. ENSO-related impacts on Antarctic sea ice: a synthesis of phenomenon and mechanisms. *Antarct. Sci.* 16, 415–425. <https://doi.org/10.1017/S0954102004002238>.
- Zhang, X., Bianchi, T.S., Cui, X., Rosenheim, B.E., Ping, C.-L., Hanna, A.J.M., Kanevskiy, M., Schreiner, K.M., Allison, M.A., 2017. Permafrost organic carbon Mobilization from the watershed to the Colville river Delta: evidence from ^{14}C ramped pyrolysis and lignin biomarkers. *Geophys. Res. Lett.* 44 (11) <https://doi.org/10.1002/2017GL075543>, 491-11,500.
- Ziegler, M., Jilbert, T., de Lange, G.J., Lourens, L.J., Reichert, G.-J., 2008. Bromine counts from XRF scanning as an estimate of the marine organic carbon content of sediment cores. *Geochem. Geophys. Geosystems* 9. <https://doi.org/10.1029/2007GC001932>.
- Zondervan, A., Hauser, T.M., Kaiser, J., Kitchen, R.L., Turnbull, J.C., West, J.G., 2015. XCAMS: the compact ^{14}C accelerator mass spectrometer extended for ^{10}Be and ^{26}Al at GNS Science, New Zealand. *Nucl. Instrum. Methods Phys. Res. Sect. B Beam Interact. Mater. At.* 361, 25–33. <https://doi.org/10.1016/j.nimb.2015.03.013>.